Review paper

Research on GNSS positioning and applications in Poland in 2019–2022

Jacek Paziewski[1*], Tomasz Hadas[2], Witold Rohm[2], Pawel Wielgosz[1]

[1]University of Warmia and Mazury, Olsztyn, Poland
e-mail: jacek.paziewski@uwm.edu.pl; ORCID: http://orcid.org/0000-0002-6033-2547
e-mail: pawel.wielgosz@uwm.edu.pl; ORCID: http://orcid.org/0000-0002-5542-1481

[2]Wroclaw University of Environmental and Life Sciences, Wroclaw, Poland
e-mail: tomasz.hadas@upwr.edu.pl; ORCID: http://orcid.org/0000-0002-4409-5078
e-mail: witold.rohm@upwr.edu.pl; ORCID: http://orcid.org/0000-0002-2082-6366

*Corresponding author: Jacek Paziewski, e-mail: jacek.paziewski@uwm.edu.pl

Abstract: This paper reviews the key studies concerning GNSS positioning and applications conducted at leading Polish research institutions from 2019 until 2022. The review also constitutes a contribution to the national report of Poland for the International Union of Geodesy and Geodynamics (IUGG) presented at the 28th General Assembly of IUGG held in 2023 in Berlin, Germany. In particular, we discuss the advances in theory and applications of relative and absolute positioning, troposphere and ionosphere sounding, smartphone and low-cost GNSS data processing, and other specific studies such as those on satellite antenna calibration and clock stability. In light of these recent advances by the Polish scientific community, continuous progress in GNSS theory and processing algorithms is thought to be maintained in the future, and GNSS applications are expected to continue to proliferate.

Keywords: GNSS, positioning, geodesy, troposphere, ionosphere

1. Introduction

GNSS now plays a vital role in providing position-related information and in Earth and environmental studies by exploiting advances in theories and cutting-edge processing algorithms, satellite deployment, the precision of new signals, and multi-sensor fusion. This progress has led to a significant spread of GNSS to new fields of science and industry, bringing further benefit to society. As a result, with GNSS, it is now feasible

to support a broad scope of applications ranging from personal and vehicle navigation through geodesy and surveying to geohazard and atmosphere monitoring.

This paper offers a review of the recent advancements by the Polish geodetic community in GNSS positioning and applications and an outline of possible future developments. This review also constitutes a contribution to the national report of Poland for the International Union of Geodesy and Geodynamics (IUGG) covering the period of 2019–2022 and presented at the 28th General Assembly of the IUGG held in 2023 in Berlin, Germany. In particular, we give credit to the most important and latest articles by Polish research institutions, which approach a wide range of GNSS studies, such as enhancing functional, stochastic, and correction models of positioning, structural health and seismicity monitoring, troposphere and ionosphere sounding, and geodynamics studies (Fig. 1). All the commented articles exhibited high novelty and research standards and were published in leading scientific journals in the field. Therefore, we anticipate they will foster meaningful scientific and technological progress and outreach geodetic-related studies.

Fig. 1. Word cloud of the topics discussed in this review paper

2. Advances in GNSS positioning

The Polish geodetic research community has recognizable achievements in developing, assessing, and applying precise positioning methods based on GNSS systems. In this regard, we distinguish the studies taking the employed positioning technique as a criterion. Consequently, below, we report the recent progress in relative positioning, including Real Time Kinematics (RTK) and Precise Point Positioning (PPP) modes.

2.1. Progress in relative positioning

Relative positioning has proved its exceptional accuracy and reliability among GNSS positioning techniques. Despite its high performance, still, noticeable progress has been recently made. This section discusses the studies on Integer Ambiguity Resolution (IAR)

algorithms, correction, stochastic and functional models of relative positioning, which foster further development in the field.

Studies on integer ambiguity resolution and validation

MAFA is the method for IAR developed at the University of Warmia and Mazury in Olsztyn (UWM). Recently, a few noticeable advances in this regard have been introduced. A search procedure has been improved by optimizing a search step. In Cellmer et al. (2022a), the authors analytically derived the search step's length for a given satellite configuration. The upper limit of the search step's size is individual for each satellite configuration. This improvement reduces the number of necessary candidates needed to find the correct solution compared to the case with fixed search steps used to date. The authors described their method using a concept of the Voronoi cells in three-dimensional space.

A reduction based on decorrelation was, in turn, proposed in Cellmer et al. (2022b) to improve the MAFA method further. The reduction process transforms the original math model into an equivalent one in the sense of obtaining the same solution. Such a reduction aims to increase the efficiency of searching for some parameters, i.e., integer ambiguities. Experiment results show a positive impact on search process efficiency, as computational time is reduced by more than 40% when processing short sessions.

Further advances were related to enhancing IAR in instantaneous relative GNSS positioning. The iterative Tikhonov regularization for single-epoch positioning was demonstrated in Fischer et al. (2022). This approach considers a single regularization parameter that regularizes baseline components and ambiguities. The precision of float solutions was improved at the cost of a small amount of regularized bias. Therefore, the overall accuracy was superior in the sense of mean-squared error. Due to the better accuracy properties of the float solution, the success probability of correct integer ambiguity estimation was higher. As a result, instantaneous precise relative positioning was more frequently guaranteed.

Despite the abovementioned progress in integer ambiguity resolution methods, a reliable validation of this step is still an issue. This task is typically accomplished with the use of hypothesis testing. From the statistical point of view, however, this approach is not rigorous in the case of multiple outliers, as it suffers from statistical dependencies between test statistics, especially in the case of baseline GNSS observations which are strongly correlated. A particular problem of the model validation using a hypothesis testing approach is the arbitrary choice of significance level – false alarm rate. In the paper by Nowel et al. (2021), a new approach that overcomes the hypothesis testing issues was presented. It uses combinatorics and information criteria (IC) from information theory. The experiments revealed that the hypothesis testing approach achieved the highest success rates of model validation when no outlier existed. However, as the number of outliers increased, the IC approach achieved the highest success rates. The validation of relative GNSS observation models using the suggested IC approach turned out to be a valuable alternative to the conventional hypothesis testing approach and, thus, deserves further investigation.

Enhancing functional, stochastic, and correction models of relative positioning

Ionospheric disturbances imply precise positioning performance to a great extent. Even in the case of Network RTK (NRTK) positioning, this unfavorable effect cannot be fully mitigated by providing network ionospheric corrections. Under disturbed ionospheric conditions, the corrections suffer from poor accuracy and the presence of outliers. These effects are driven by a failure of a spatial interpolation process. RTK positioning becomes even more challenging in the case of a long-range scenario when baselines often exceed 100 km.

In Paziewski and Sieradzki (2020a), the authors proposed and examined the method allowing for precise wide-area rapid static and RTK positioning under severe ionospheric conditions. The method enhances the relative positioning model by combining multi-constellation network ionospheric corrections and a new algorithm eliminating the changes of the ionospheric delays in time. The method's performance was validated using GPS, BDS, and Galileo observations collected at high latitudes during the ionospheric storm on August 25–26, 2018. As expected, the poor accuracy of the network ionospheric corrections and, consequently, a decline in RTK performance with routine relative positioning model were confirmed. On the contrary, with the novel method, it was feasible to achieve a remarkable improvement in the ambiguity resolution domain, which reached even over 20% compared to the benchmark models.

The studies on enhancing Network RTK positioning were also conducted at the Department of Geodesy and Geodetic Astronomy Warsaw University of Technology (WUT). In Prochniewicz et al. (2020), the authors comprehensively analyze the performance of all RTK services provided by Poland's nationwide networks of Continuous Operating Reference Stations (CORS). The tests covered 15 Network RTK services and 7 RTK services from the ASG-EUPOS, SmartNet, TPI NetPro, VRSNet, and NadowskiNet networks. The accuracy and reliability of positioning performance, time to first fix, correction average age, and compliance of the reference frame realization were investigated. Table 1 exhibits position accuracy with Root Mean Square Error (RMSE) and standard deviation (STD) for tested services as an average value for each network. The results revealed that accuracy and precision for all NRTK and RTK services for the horizontal component were at very similar levels of 1 cm for RMSE and up to 1 mm for STD. The only exception is the NadowskiNet network, for which the RMSE for the NRTK service reached 2 cm. Regarding the height component, the accuracy of NRTK and RTK ASG-EUPOS services are two to three times less accurate than other networks with an RMSE of 4 cm.

Much attention has also been paid to refining the stochastic models of GNSS positioning. A new multi-constellation and multi-signal empirical stochastic model was proposed as a fully populated variance-covariance (VC) matrix. The model considers the Carrier-to-Noise density Ratio (C/N0)-dependent variance function and the cross- and time-correlations between the observations (Prochniewicz et al., 2021). The validation of the novel stochastic model against the common elevation-dependent one showed that the former increases both the positioning accuracy and the efficiency of ambiguity resolution. Figure 2 summarizes the position error of two comparative weighting methods: the elevation-dependent model and the C/N0 model, with the individual empirical model

Table 1. Mean positioning accuracy and precision reflected in RMSEs and STDs for tested networks (Prochniewicz et al., 2020)

Method	Network	RMSE [m]		STD [mm]		
		Hor.	Vert.	North	East	Height
NRTK	ASG-EUPOS	0.010	0.027	0.61	0.44	1.12
	SmartNet	0.009	0.009	0.61	0.42	0.96
	TPI NetPro	0.012	0.018	0.53	0.35	1.21
	VRSNet	0.012	0.017	0.63	0.44	1.21
	NadowskiNet	0.022	0.009	0.52	0.37	0.86
RTK	ASG-EUPOS	0.011	0.036	0.76	0.57	1.29
	SmartNet	0.011	0.012	1.11	0.61	1.82
	TPI NetPro	0.011	0.021	0.68	0.45	1.30
	VRSNet	0.011	0.018	0.65	0.47	1.78

for each satellite block taking into account the correlation parameters. The 3D position error statistics are shown as a box whisker plot with the 75th, 50th, and 25th percentiles of errors and most extreme values. In addition, a red dot marks the maximum position error for each scenario. These statistics confirmed the effectiveness of the C/N0 model in reducing errors, for which the optimal solution was obtained for the multi-GNSS model (GREC) with a median error of 4.3 mm and the lowest maximum error of 15.2 mm.
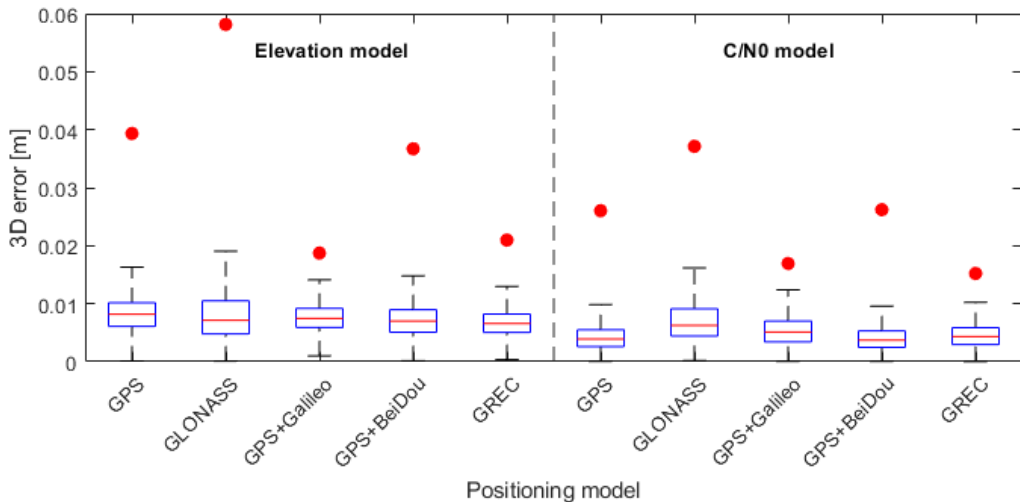
Fig. 2. Positioning error statistics for different stochastic models and system combinations

Research on stochastic properties of GNSS signals also included a complex analysis of the noise type in double-differenced GNSS observations using three statistical tools: Autocorrelation Function (ACF) method, the Lomb–Scargle (L–S) periodogram method,

and the Allan variance (AVAR) method (Prochniewicz et al., 2022). The methods allow identifying different noise characteristics for different types of observations. As experiment results revealed, the lowest noise of code measurements characterized the GPS C5Q and Galileo C7Q/C8Q observations, with an STD of about 10 cm. The noisiest were the GLONASS C1C and C2C signals, with 90 cm and 45 cm STDs, respectively. The carrier-phase observations, in turn, were characterized by a comparable noise of 1–3 mm. The ACF analysis showed that the double-differenced carrier-phase observations could be considered uncorrelated for the 1-second interval data, while for the code observations, this interval increases to 20 seconds. Based on the Modified Allan deviation method, the noise type for GPS and Galileo carrier-phase observations was identified as a white phase modulation one. In contrast, a white or flicker noise was found for the GLONASS signals depending on the integration step.

The following studies considered the multipath impact on GPS and Galileo code and phase observations. The analysis was performed using code and carrier-phase observations combination, double differences of carrier-phase observations, and wavelet transform (Prochniewicz and Grzymala, 2021). It was shown that Galileo code observations are more resistant to multipath and measurement noise than GPS ones (Fig. 3). The maximum impact of multipath on code observations was even a meter higher for the GPS C/A code than the E1 civil code of Galileo. The impact of multipath on phase measurements was similar for both systems, at a few millimeters.
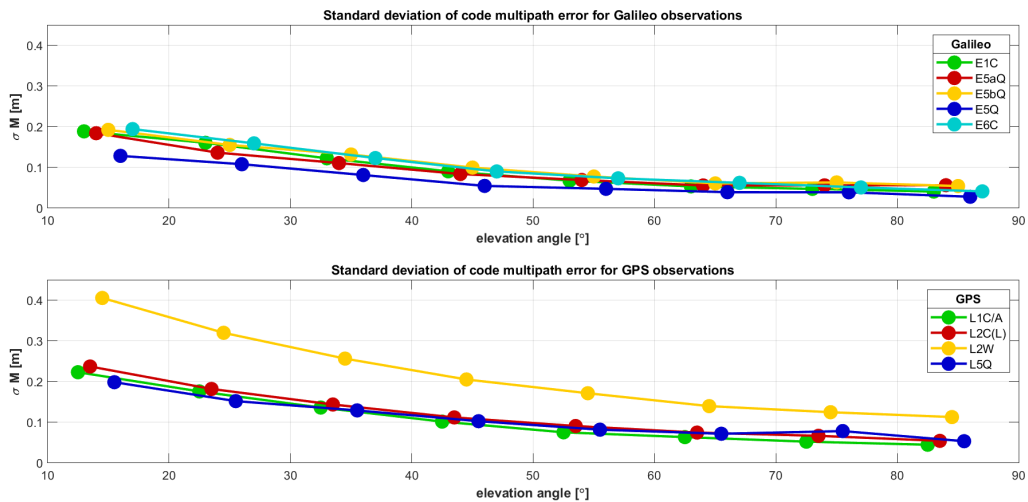
Fig. 3. Multipath error for code observation: Galileo (top) and GPS (bottom)

2.2. *Progress in Precise Point Positioning*

The studies by the Polish scientific community related to the Precise Point Positioning technique considered, among other topics, the impact of emerging GNSS, such as Galileo and BeiDou, the monitoring of orbit and clock products, including real-time corrections,

refining functional and stochastic models of positioning, and the analysis of static and kinematic positioning in various applications.

Hadas et al. (2019) analyzed the performance of absolute positioning with the fully serviceable Galileo constellation. It was noticed that despite two empty slots in the Galileo constellation, the maturity of the Galileo space segment already allowed for the worldwide Galileo-only positioning. It was demonstrated that few-decimeter horizontal accuracy is achievable by processing Galileo pseudoranges and broadcast ephemeris in a static mode, which is superior to the corresponding GPS standard positioning service (SPP). A sub-decimeter horizontal accuracy for both GNSS was achieved when broadcast ephemeris was replaced with real-time products from the Centre National d'Études Spatiales (CNES). It was noticed that the high stability of the Galileo onboard clocks allows performing PPP with broadcast ephemeris leading to remarkable accuracy in the daily static solution, i.e., RMSE of 0.07 m and 0.10 m for the horizontal and vertical components, respectively. Compared to GPS-only positioning, this improved by a factor of 3 and 2, respectively. In the kinematic mode, the improvement with respect to GPS was 15% and 4%, respectively.

The impact of the GNSS constellation development on the PPP performance was also investigated at the Military University of Technology in Warsaw (MUT). In Kiliszek and Kroszczynski (2020), the authors used GPS, GLONASS, and Galileo measurements from one week of consecutive years, i.e., 2017, 2018, and 2019. In the following years, the increasing influence of the Galileo system was noticed, where already in 2019, positioning using only this system was possible. In addition, Galileo-only positioning precision obtained a 50% improvement in 2019 compared to 2017. The best results were obtained for GPS+GLONASS+Galileo in 2019, which was strongly influenced by the development of the Galileo system, but the use of GPS still had the most significant impact. GPS-based PPP performance still outperformed GLONASS-only and Galileo-only, and even than GLONASS+Galileo. A triple-system solution allowed for achieving high accuracy with 90% availability even with an elevation angle of 40°.

In Zajdel et al. (2022), the authors compared GNSS station coordinates' precision and spectral content determined using GPS, GLONASS, and Galileo constellations. The recent development of the Galileo, GLONASS, and BeiDou systems allowed for evaluating incompatibilities resulting from using different constellations and highlighted the benefits and consequences of using individual GNSS and multi-constellation observations. It was found that each system introduces significant changes to the measured coordinates, with magnitudes of up to several centimeters. The researchers identified a particular group of signals unique to each GNSS system, called the orbital artifact group, which causes inconsistencies in station coordinate series. These signals were demonstrated by analyzing 2-year data from fifteen globally distributed stations using the PPP technique. Galileo has the most dominant orbital artifacts with periods of 14.08 h, 17.09 h, 34.20 h, 2.49 d, and approximately 3.4 d, while GLONASS has analogous signals with periods of 5.63 h, 7.36 h, 10.64 h, 21.26 h, 3.99 d, and about 8 d. GPS orbital signals appear with periods that correspond to the satellite ground track repeat period and its harmonics. These harmonics coincide with the solar tide K1 (23.93 h), resulting in inconsistencies between GPS-based analyses and tidal geophysical models, which can reach an average

of 12 mm for the ocean tide K2 (12.97 h) in the height component of station coordinates. Finally, the authors outlined that the amplitude of the orbital signals varies for different station locations and depends on the geometry of GNSS observations and the dominant direction of satellite overflights. Using a combination of GPS and Galileo provides a 10% increase in station coordinate precision compared to using the best-case single system solution based on Galileo observations.

Due to the increasing interest and utilization of real-time PPP services, much attention was paid to analyzing the quality of real-time corrections. Kazmierski et al. (2020) investigated the quality of real-time quad-system orbit and clock corrections provided by CNES over three years (2017–2019). The reported availability of corrections increased to 95% during 2019, with some issues related to individual GLONASS and Galileo satellites, as well as to geostationary BeiDou satellites. The accuracy of products was assessed with respect to CODE final products and expressed in terms of the Signal In Space Range Error (SISRE). For GPS and GLONASS, SISRE usually remained below 2 cm and 10 cm, respectively, over the entire test period. A clear evolution of Galileo products was noticed, and since 2019, they occurred to be superior even to GPS products. For BeiDou, the SISRE also changed over time, but since 2019 it has remained at the 5 cm level. It was shown that the accuracy of real-time products depends on the GNSS, satellite block, onboard atomic clock, and sun elevation above the orbital plane. Finally, independent validation of real-time orbits was performed with satellite laser ranging (SLR). The number of outliers in the real-time products was found, thus indicating that despite the high quality, these products are still not as robust as expected.

Pelc-Mieczkowska and Tomaszewski (2020), in turn, evaluated real-time products from four different analysis centers, aiming at the representative evaluation of state-space representation (SSR) products. It was noted that the magnitude of the orbital residuals with respect to a reference orbit was similar for each real-time product. Still, streams performed differently over time due to various strategies applied in the processing software. More significant differences between SSR products were noticed in the clock accuracy, from 2 cm to over 10 cm. To evaluate the impact of these products on positioning performance, PPP and SPP results were derived from GPS data. Two streams, i.e. CLK90 and CLK50 were identified as those providing the highest accuracy in the PPP mode, i.e. 5 cm, 7 cm, and 11 cm for the North, East, and Up components, respectively. All SSR products improved the accuracy of code-only positioning by a factor of 3.5.

The following studies were aimed at enhancing the stochastic models of PPP. In this regard Kiliszek et al. (2022) analyzed the impact of using various weighting functions of GPS and Galileo observations. Calculations were made for GPS-only, Galileo-only, and GPS+Galileo using eight different weighting functions. For GPS-only, the best results were obtained for a different function than for Galileo-only. In contrast, the best function for Galileo-only was the one for which the observations at lower elevation angles assumed higher weights than for GPS. The best results for the GPS+Galileo solution were obtained using two different weighing functions depending on the constellation. It was noticed that the choice of the weighting function had a particular impact on the Up coordinate component and a significant impact on the tropospheric delay and the convergence time.

As the ionosphere remains the primary error source in absolute GNSS positioning, it must be handled carefully in PPP. The first-order ionosphere delay is typically eliminated by forming an ionosphere-free linear combination. Alternatively, ionospheric delays can be parametrized and estimated when undifferenced and uncombined observations are processed. Paziewski and Sieradzki (2020b) investigated both functional models of PPP and concluded their equivalent performance, providing that corresponding stochastic models are also applied. Furthermore, Poniatowski and Nykiel (2020) investigated the impact of Medium-Scale Traveling Ionosphere Disturbances (MSTIDs) on the kinematic PPP. This case study considered the strongest geomagnetic storm of the 24th solar cycle, with the geomagnetic activity index reaching –223 nT. The MSTIDs caused numerous cycle slips, which reduced the number of satellites considered in positioning. As a result, significant accuracy degradation was noticed at all analyzed stations, and for some epochs, the number of available satellites was insufficient to determine the position. The authors claimed that receivers struggle with correct phase tracking during an MSTID.

The worth-mentioning results were also achieved in the field of geodynamic applications of PPP. Pelc-Mieczkowska (2020) aimed to determine the uncorrelated trends in the coordinate time series derived with PPP. Seven-year long time series of daily solutions of nine permanent stations were considered. The accuracies of the obtained trends were better than 0.1 mm, thus legitimating the PPP technique for geodynamic studies. Dawidowicz (2019) in turn, analyzed position determination accuracy from 30-minute GPS and GLONASS observation sessions using the PPP technique. Previous research in this area has mainly focused on more extended time frames, where observation sessions ranged from 1 to 8 hours. The analysis was based on 30 days of GNSS observations recorded at eight permanent stations of the ASG-EUPOS system in Poland. Post-processing was performed in the NAvigation Package for Earth Orbiting Satellites (NAPEOS) software in five scenarios considering single-GNSS and dual-GNSS processing and a float or fixed ambiguity resolution for GPS. Individual antenna phase center corrections (PCC) values were used to correct observations. It was revealed that the sub-hourly PPP technique could provide an accuracy of 0.5 cm for the horizontal position components and 1 cm for the vertical position component. Such accuracy characterized the solutions where GPS and GLONASS observations were used in the multi-station PPP approach (fixed ambiguity solution). Similar results were also obtained for two other scenarios: GPS-only with ambiguity fixing and the GPS/GLONASS scenario with float ambiguity solution. GPS-only and GLONASS-only with float ambiguities resulted in an accuracy of 1 cm and 2 cm for horizontal and vertical components, respectively.

Finally, a practical application of PPP was reported in (Krasuski and Wierzbicki, 2021). The authors developed a method of determining an aircraft's position based on the PPP technique that uses a weighted mean of positions determined with GPS-only and GLONASS-only processing. An airborne experiment was carried out with a dual-frequency GNSS receiver on board, and the online CSRS-PPP software was used for the processing. Obtained positions were validated against the RTK solution. An improvement of 11% to 87% was obtained by weighting the single-GNSS solutions. The model was also implemented in the RTKLib software, and the corresponding improvement varied from 45% to 82%.

3. Troposphere studies with GNSS

Between 2018 and 2022, a significant number of articles were published by Polish re-search teams, some in collaboration with international researchers affiliated to institutions in countries such as Luxembourg, Bulgaria, Italy, France, Germany, Netherlands, Portu-gal, Belgium, Czechia, Austria, Switzerland, Taiwan, USA, China, Iran, and Australia. These papers were published in internationally recognized journals thematically linked with remote sensing, GNSS processing and applications, geophysics, the Earth system and the atmosphere.

The literature review revealed that topics that are of interest to the Polish GNSS remote sensing research community are related to: increasing the capabilities and capacities of ground-based GNSS products, developing space-based GNSS products, advancing GNSS tomography, monitoring and investigating climate change using GNSS sensors, investigating severe weather case studies with GNSS, moving even further by using GNSS observations in numerical weather models and nowcasting.

3.1. Ground-based GNSS products

Within this topic, the authors studied the GNSS troposphere products using post-processing (Stepniak et al., 2022), near real-time (Tondas et al., 2020) and real-time mode (Hadas et al., 2020; Hadas and Hobiger, 2021) with both relative and Precise Point Positioning approaches.

Stepniak et al. (2022) evaluated the performance of GNSS tropospheric post-processing estimates derived from IF PPP and the relative mode. The study also aimed to evaluate the impact of some GNSS data processing aspects on the quality of the derived ZTD series for climate applications. Three following scientific questions were discussed in this research: 1) Does the PPP technique generate fewer outliers than DD processing? 2) What is the impact of orbit & clock products on the accuracy of ZTD estimates us-ing the PPP technique? 3) How does ambiguity resolution impact ZTD estimates in the PPP solution? The results showed that the ZTD time series obtained from DD solutions contained more outliers with larger magnitudes than estimates from PPP solutions. The sensitivity tests of ZTD estimates to the satellite products, the ambiguity resolution, and the mapping functions indicated that PPP solutions were superior to the DD results. The latter showed larger biases and excessive noise, partly due to datum effects, compared to ERA5 reanalysis. It was demonstrated that changing the mapping function has a signif-icant impact, with VMF1 being superior to GMF, mainly found at a time scale longer than one day, which is not adequately represented in GMF. The impact of ambiguity resolution on the ZTD estimates in PPP mode was found to be small, mainly because the satellite products are determined from ambiguity-fixed processing of the global IGS network, transferring the information to the PPP solution.

Over the past decades, the Near Real-Time (NRT) processing of GNSS troposphere estimates has been continuously improved; however, the standard processing strategy was based on an hourly calculation interval. Tondas et al. (2020) investigated a new

ultra-fast GPS data processing (NRT UF) service to obtain troposphere parameters and coordinates with a 15-minute latency (Fig. 4). The NRT UF system was designed to collect the GNSS observations and products in the first minute of each quarter hour. The remaining 14 minutes were dedicated to the estimation process in Bernese GNSS Software v. 5.2. To assess the quality of the NRT UF solution, the independent GNSS post-processing service, the official EUREF solution, and radiosonde observations were used. The quality analyses demonstrated that the standard deviation of the zenith total delay (ZTD) was at level 5–10 mm for co-located GNSS and radiosonde locations. An evaluation of the coordinates obtained from the 15-minute NRT UF processing indicated the RMSE of the Helmert transformation of 2.2 mm with respect to the post-processing data sets. The newly investigated methodology of the NRT UF service may be applied for short-term weather forecasts and ground deformation monitoring.
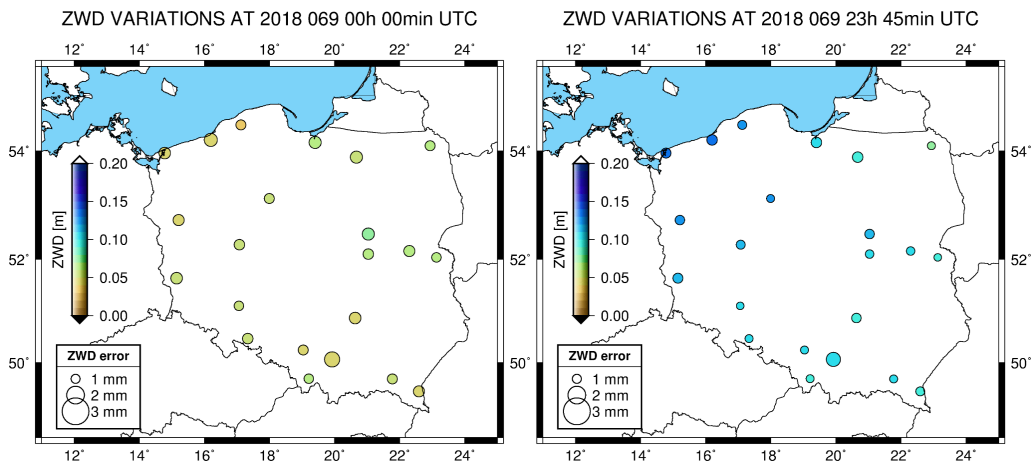
Fig. 4. Zenith Wet Delay values and errors estimated by NRT UF service from 069 DOY 2018 at 00:00 UTC and 23:45 UTC

Hadas et al. (2020) investigated various strategies for real-time ZTD estimation and the impact of processing parameters on the accuracy of troposphere products, including horizontal gradients. The following aspects were considered: PPP functional model, GNSS selection and combination, inter-system weighting, elevation-dependent weighting function, and gradient estimation. A cosine-type elevation-dependent weighting function was proposed. An advanced strategy dedicated to real-time GNSS meteorology was defined as follows: multi-GNSS undifferenced and uncombined processing with inter-system weighting using SISRE (Kazmierski et al., 2018) and gradient estimation. It allowed estimating ZTD with accuracy ranging from 5 to 10 mm. Compared to the common approach in real-time GNSS meteorology, i.e., GPS-only processing using ionosphere-free linear combinations, the advanced strategy improved the accuracy of ZTD by 17% and its uncertainty by over 40%. Moreover, it was demonstrated that the maturity of all four GNSS and corresponding real-time orbit and clock products allowed for providing single-system GNSS ZTD, but with varying accuracy. Further

studies analyzed the benefits of the fully serviceable Galileo constellation for real-time meteorology (Hadas and Hobiger, 2021). Although Galileo and supporting services were already reliable, and Galileo has many advantages over other GNSS, including GPS, the Galileo-only real-time ZTDs were less accurate than GPS only-products. The superior results were obtained by combining both GNSS, which led to improved accuracy with respect to IGS and EPN products by up to 8.5%. For EPN stations, the 5 mm accuracy of ZTD was achieved (Fig. 5). Moreover, GPS+Galileo solutions were free from orbit-related artificial signals of high frequency. The abovementioned achievements legitimate real-time ZTD products for assimilation in numerical weather prediction (NWP) models.
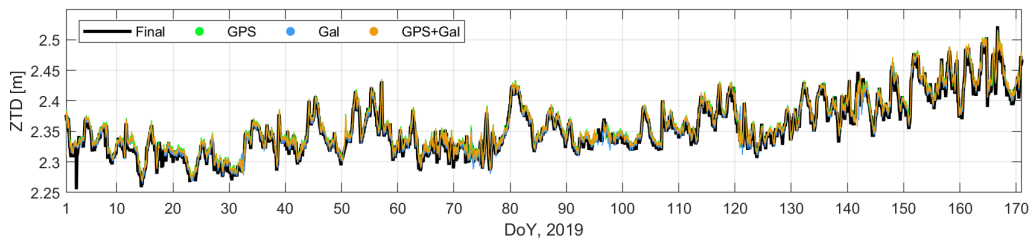
Fig. 5. Time series of real-time ZTD from GPS, Galileo, and GPS+Galileo solutions compared to the IGS Final products; station WROC, DoY 1-170, 2019

Further developments of GNSS real-time troposphere monitoring capabilities for small-scale atmosphere variability were discussed in Marut et al. (2022). Authors used in-house developed low-cost dual-frequency GNSS receivers and validated the possibility of observing changes in integrated water vapor (IWV) content in the atmosphere on the local scale. For this purpose, they recorded two weeks of multi-GNSS data with a low-cost station and compared results with the co-located IGS station WROC and the water vapor radiometer. Analysis showed that standard deviations of IWV differences were 1.0 kg/m^2 and 1.5 kg/m^2 for post-processing and real-time products, respectively. Moreover, the authors set up a city-scale network of 16 low-cost receivers in and around Wroclaw, Poland. It was noticed that the IWV time series among stations were relatively consistent. The standard deviation of IWV differences between low-cost GNSS and other sources remained below 1.5 kg/m^2. Still, significant inter-station differences up to 16 kg/m2 were observed, as well as temporal disagreements with the high-resolution numerical weather model WRF ranging from –12 to +11 kg/m^2 (Fig. 6). Therefore, local-
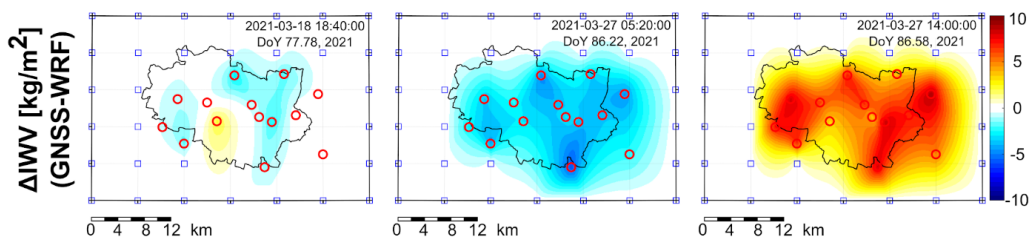
Fig. 6. Small-scale IWV variations with respect to the WRF model

scale IWV dynamics were captured for the first time using in-situ measurements, i.e., the network of low-cost GNSS receivers.

3.2. Space-based GNSS products

The space-based neutral atmosphere GNSS processing capabilities were developed by Hordyniec et al. (2019). Authors developed in-house radio occultation (RO) processing software to process the level-1 excess phase delay data from most satellite-based GNSS receivers such as Constellation Observing System for Meteorology, Ionosphere and Climate (COSMIC-1 or 2). The full processing cycle was established from excess phase observations to refractivity, temperature, and water vapor profiles. The comparison between retrieved refractivity profiles and radiosonde profiles shows discrepancies up to 5% of root mean square error. The results were also validated with official products processed at COSMIC Data Analysis and Archive Center (CDAAC), showing only slightly worse performance.

Further use of space-based RO profiles was investigated in Lasota (2021). The author followed a trend to exploit artificial intelligence in GNSS space-based meteorology. In the usual approach, refractivity profiles are combined with the external information from weather models through a one-dimensional variational scheme to determine a one-dimensional tropospheric state in a statistically optimal way. To overcome the dependency on the auxiliary meteorological parameters, the author trained four different models, namely artificial neural network and random forest algorithms accepting refractivity or bending angle as an input to obtain vertical profiles of temperature, pressure, and water vapor. The tests agreed well with the background ERA5 information and the official wetPf2 of the COSMIC Data Analysis and Archive Center. The vertically averaged RMSEs were around 1.7 K for the temperature, 1.4 and 0.45 hPa for total and water vapor pressure, respectively. Further validation with the radiosondes revealed slightly worse results, with the largest discrepancies visible in the lower troposphere below 5 km altitude.

3.3. GNSS tomography

Polish research teams have been intensively investigating GNSS tomography models (Fig. 7) since the initial research nearly 15 years ago (Rohm and Bosy, 2009). One of the cornerstone papers was published by Brenot et al. (2019), who summarised the efforts of the IAG's Working Group on GNSS tomography. This study aimed to revise and compare the methodology of GNSS tomography by using GPS data from the Australian CORS network during a severe weather event. Sensitivity tests and statistical cross-comparisons of tomography retrievals with independent observations from radiosonde and radio-occultation profiles demonstrated the effectiveness of the presented methodology. The initial conditions and the use of data stacking and pseudo-slant observations are critical to GNSS tomography. The best strategy can reduce the normalized RMSE of the tomography

solution by more than three compared to radiosonde estimates. Data stacking and pseudo-slant observations can also significantly improve tomography retrievals, resulting in a normalized RMSE improvement up to 17% in the 0–8 km layer. The study highlights the importance of evaluating tomography retrievals against independent measurements and estimating the quality of weather forecasts. Finally, a comparison of multi-model tomography with NWP demonstrates the potential of tomography retrievals for enhancing our understanding of severe weather conditions.
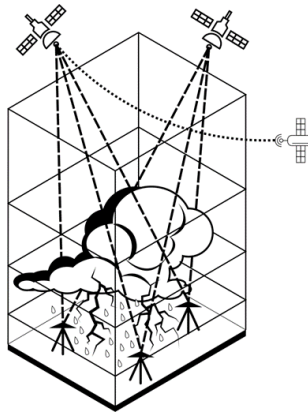
Fig. 7. Concept of GNSS tomography model that is sensing severe weather events using intersecting GNSS signals

GNSS tomography domain optimization and apriori data were identified in Haji-Aghajany et al. (2020) as two of the most promising advancements. This study proposed a new tomography approach that optimized the number of voxels and incorporated constraints to improve the spatial resolution of tomography. The accuracy of the obtained water vapor estimates was validated using radiosonde observations and GPS positioning results. Comparing the results with radiosonde observations, it was found that incorporating the WRF model outputs and topography information reduces the RMSE by 0.803 g/m^3. Furthermore, the validation using GPS positioning data shows that under wet weather conditions, incorporating WRF model outputs and topography information reduces the RMSE of the east, north, and up components by approximately 17.4, 10.5, and 20.0 mm, respectively, which corresponds to reductions of 46%, 36%, and 54%. A similar study was performed by Adavi et al. (2020). The authors claimed that the parameterization method used for computing the design matrix could affect the accuracy of the resulting model. This paper examined the impact of two different methods, the straight-line and ray-tracing methods, on the accuracy of computed ray lengths passing through model elements. Additionally, the effect of including topography in the tomography model was investigated. Radiosonde measurements from the COST benchmark dataset were used to validate the model's accuracy. The results indicated that the Eikonal ray-tracing method, with or without topography, produces more accurate wet refractivity estimates than other methods. The mean RMSE values for wet refractivity estimates using

the Eikonal ray-tracing method were 1.313 and 1.766 ppm, respectively, for models with and without topography compared to radiosonde profiles.

To further investigate the preconditions to the final GNSS tomography retrieval quality, Adavi et al. (2022) proposed using the concept of matrix resolution spread. The authors tested this method on two synthetic and one real dataset covering overlapping periods in Germany and Czechia in 2013. Results showed a strong correlation between the spread and the standard deviation of the reconstructed wet refractivity and a significant correlation with the bias of the retrieved field. Thus, the spread of the resolution matrix can serve as a proxy for the accuracy of the tomography reconstruction field based on the quality of the observations, the initial field, and the design matrix.

The introduction of real-time and near real-time high-quality troposphere products motivated the researchers to look into real-time GNSS tomography retrievals. Sá et al. (2021) introduced a new tomographic system called SEGAL GNSS Water Vapour Reconstruction Image Software (SWART). The method utilizes parallelized algebraic reconstruction techniques (ARTs). It is faster than other implementations, making it possible to estimate water vapor for larger GNSS networks and for near real-time weather predictions. The potential of SWART was demonstrated using data from 26 stations in Poland over 56 days. The estimated water vapor from SWART showed good agreement with radiosonde solutions, with a mean RMS of 1.5 g/m^3 for lower layers and an overall improvement of 5% until the layer 6750 m compared to the WRF atmospheric model. Additionally, rapid and strong variations in water vapor observed by radiosondes were detected by GPS tomography but not modeled by the WRF.

Another exciting use of GNSS tomography was demonstrated by Haji-Aghajany et al. (2021), who, for the first time, introduced the GNSS tomography model in positioning. This study used GNSS stations under different weather conditions to investigate the effect of function-based and voxel-based tropospheric tomography methods on positioning accuracy in static and kinematic modes. After validating the results of tomography methods using radiosonde observations, the tomography-based positioning solutions were compared with the positions obtained using tropospheric models. Results showed that the accuracy increases when applying tomography approaches, particularly with the use of function-based tropospheric tomography. The function-based method can improve the up component of the static and kinematic modes by approximately 0.4 and 0.8 cm, respectively, compared to the voxel-based method. Moreover, the function-based tropospheric tomography reduces the convergence time of the kinematic PPP solution.

3.4. GNSS troposphere estimates in climate change

The GNSS observations are stable over long periods, with little to no calibration and verification needed. Therefore a clear interest in climate research was also identified in the publications authored or coauthored by Polish researchers. One of the fundamental studies related to the usability of the GNSS troposphere time series was published by Yuan et al. (2021). The authors evaluated the use of the newly published dataset from the fifth-generation European Centre for Medium-Range Weather Forecasts (ECMWF)

atmospheric reanalysis (ERA5) to analyze climate change in Europe. For this purpose, they determined time series trends of IWV values and compared them with IWV trends determined from GPS observations for 109 permanent stations operating in the period 1994-2019. The authors showed that the commonly used nature of the series that does not consider the internal temporal correlation is unsuitable for describing the above series. Consequently, the appropriate model to reliably describe the nature is the ARMA(1,1) model. Using the erroneous nature of the series leads to an underestimation of the error values of the determined IWV trends and thus affects the interpretations in terms of climate.

Another study that looked at the GNSS time series was the one published by Van Malderen et al. (2020). The authors tested the effectiveness of algorithms commonly used to homogenize tropospheric time series. They used three training data sets for this purpose, named easy, moderate, and complex, each consisting of 120 time series that differed in the nature of the series and the number of jumps. Participants in the experiment did not know the true epochs of the jumps. The investigation showed that most methods underestimate the number of breaks and have a significant number of false detections, which can significantly affect the trend values determined from tropospheric series and thus lead to erroneous climate interpretations.

Both studies (Van Malderen et al., 2020; Yuan et al., 2021) highlighted a need for careful investigation of GNSS troposphere estimates before use in climate trend estimation. Such successful trend investigations were performed for the global tropics (Baldysz et al., 2021) and Poland (Araszkiewicz et al., 2021). Baldysz et al. (2021) have investigated the possibility of using GNSS IWV time series to monitor atmospheric moisture variability related to the various climate modes. They have used 18 years of GNSS IWV time series from International GNSS Service (IGS) stations located in global tropics and applied singular spectrum analysis (SSA) to estimate non-linear trends. Results showed that climate modes on different time scales were visible in long-term GNSS IWV variability. Both global and regional climate patterns were reflected in the analyzed time series. The largest number of stations were correlated to the El Nino Southern Oscillation (ENSO), with a maximum cross-correlation coefficient between GNSS IWV and Multivariate Enso Index equal to 0.78. However, smaller scales (compared to the ENSO) climate phenomena, expressed by the, e.g. Dipole Mode Index, Hawaii index, Caribbean index, or North Pacific Gyro Oscillation index, were also clearly visible. The local sea surface temperature (SST), associated with mentioned climate patterns, was investigated as the main driver of integrated moisture variability over most stations. However, there were still cases of coastal stations that showed insignificant correlation to the local SST but statistically significant correlation to the e.g., ENSO, thus pointing to the strong influence of atmospheric teleconnections.

Araszkiewicz et al. (2021), in turn, determined the ZTD from more than 150 stations in Poland and the surrounding area from 2008 to the end of 2020. The study aimed to analyze multi-year changes in atmospheric precipitable water (PW). For these purposes, the ZTD was converted to PW, and temporal and spatial changes were analyzed. The mean PW value for the entire period for the Polish area was 15.05 mm, which was consistent with previous studies using meteorological data. The distribution of the PW

and their fluctuations illustrate the strong influence of the abrasion of two climatic zones. It was particularly evident in the annual PW fluctuations, where the northwestern part of Poland, tempered by the influence of the oceanic climate, showed smaller amplitudes of seasonal changes, while the continental climate influenced the eastern region. The paper also showed a positive trend of PW changes at all stations, confirmed by a systematic change in temperature in the area.

3.5. GNSS troposphere for severe weather case studies and modeling efforts

GNSS-derived ZTDs, horizontal gradients, and Precipitable/Integrated Water Vapour (PWV/IWV) are frequently employed for investigating signatures of severe weather events, such as tropical cyclones (aka hurricanes), severe storms with hail, and derechos. Moreover, some authors employ space-based GNSS profiles and raytracing to enhance understanding of severe weather phenomena. Tropical cyclones (TC) are synoptic-scale systems forming over warm oceans characterized by extremely strong winds and copious rainfalls. The potential financial losses they can cause and the risks to human safety underscore their significance. Although the correct prediction of TC tracks has improved over the years, our understanding of their structure and development remains limited. Radio Occultation (RO) meteorological profiles and GNSS ground-based observations serve as a valuable source of information about the atmosphere, improve weather forecasting, and help predict severe weather events such as tropical cyclones.

The GNSS products can also serve as an extra tool for validation, as presented in Lasota et al. (2020b). The authors used the slant total delays (STD) from 28 GNSS stations uniformly distributed over Taiwan to verify the quality of NWP and atmospheric reanalysis during the passage of tropical cyclone Meranti, which was the strongest TC in 2016. For this purpose, the STDs were reconstructed from WRF, GFS, and ERA Interim using a 2D piecewise ray-tracing algorithm and compared to GNSS retrievals. The analysis showed good agreement between GNSS and ray-traced STD with the best results for the WRF model, where the mean difference and standard deviation equaled –0.5 mm and 29.4 mm. The highest discrepancy was found for ERA-Interim reanalysis, most likely due to coarse spatial and temporal resolutions. Furthermore, the impact of hydrometeors on propagating GNSS signal was evaluated and reached an average of 2.8 mm for the WRF model and contributed to the lower errors in most cases.

Another example of a tropical cyclones study is Ejigu et al. (2021). The authors used ZTDs from 922 permanent GPS stations located on the east coast of the United States to monitor and predict the paths of two hurricanes, namely Hurricane Harvey and Irma occurred in 2017. For this purpose, ZTD values were converted to IWV values, which were then analyzed for maxima and modeled using a spaghetti plot. The authors showed that IWV values determined from GPS observations could facilitate the tracking and monitoring of hurricane activity at least several hours before the storm arrives. This is of great importance with the increasing number of hurricanes striking US coasts each year, given the incredible number of permanent GPS stations whose observations are available with little delay.

Next, Hadas et al. (2021) estimated ZTD and horizontal gradients for 160 EPN stations during the category 5 Lorenzo hurricane from September 23 to October 4, 2019. Before the hurricane was formed and after it dissipated, the magnitudes of horizontal gradients mainly remained below 1 mm and did not reveal any predominant directions. However, starting from September 24, magnitudes of gradients exceeded 3 mm in central Europe, and consistent signatures in the gradient fields were observed. Therefore it was confirmed that horizontal gradients reflect meteorological situations during severe weather events. To further leverage TC studies, Lasota et al. (2020a) comprised TC best tracks with the nearby RO profiles in the publicly available archive. The authors gathered 1822 TC best tracks and co-located them with 48 313 RO profiles, which lied 500 km and occurred within a three hour window from the TC eye. The analysis showed that the repository covers all the TC intensities and basins, which was proved by the practical example.

The most common severe weather events in Europe are storms, which could produce a number of devastating weather phenomena such as hail, copious winds, and flash floods. Most of these events are fueled by vertical instability and an excessive amount of water vapor. Both can be sensed with GNSS signals on ground and space platforms. Densely distributed ground-based stations provide accurate but averaged information about the tropospheric state above the receiver, while RO profiles have high vertical resolution and accuracy; however, their location is quasi-random and sparse. Therefore, GNSS data fusion is crucial and can provide detailed insight into the atmospheric state as presented by Lasota et al. (2022), who used combined ground-based GNSS and RO observations to study severe weather phenomena. The authors showed that two selected severe hail events, which occurred in 2014 and 2019 in Bulgaria, were characterized by a cold upper air-pool and large specific humidity anomaly between 2 and 6 km pronounced in the RO anomalies of bending angle, temperature, and humidity. Further inspection of the ERA5 integrated water vapor transport confirmed the elevated humidity in the form of the atmospheric river. The discrepancy was also visible in the ground-based observations, where the large fractional differences between GNSS and WRF tropospheric delays resulted most likely due to offset between RO and WRF humidity profiles.

Another example of using dense GNSS observation was demonstrated in Nykiel et al. (2019). Specifically, The authors analyzed a derecho event in Poland on August 11, 2017. The investigation employed GPS and GLONASS observations from 278 GNSS reference stations in Poland. With the Bernese GNSS Software ver. 5.2, the authors estimated the ZTDs and tropospheric gradients at 5 and 15-minute intervals, respectively. By integrating meteorological data from synoptic stations, PWV was retrieved, providing information about the amount of water vapor in the atmosphere. PWV, rate of PWV (ROP), and tropospheric gradient maps facilitate monitoring the derecho event. Case studies on selected GNSS stations compared PWV, reflectivity, and microwave radiometer readings. During the primary phase of the event, the authors observed the maximum PWV value of 52.1 mm at 20:30 UTC. The analysis also revealed a high correlation between PWV/ROP maps and reflectivity data derived from meteorological radars regarding the direction, speed, time, and location of the derecho event.

The efforts to improve the consistency of IWV retrieval were reported in Baldysz and Nykiel (2019). The authors developed a new model for dependency between water

vapor weighted mean temperature and surface temperature (the Tm – Ts relationship) by studying long-time series of integrated water vapor (IWV) delivered from radio-soundings (RS) across Europe. Using 24 years of RS IWV data (1994–2018), they estimated various coefficients of the Tm – Ts relationship and established models based on various synoptic terms. The accuracy of all developed models was tested using 109 RS stations. Results showed that the best accuracy was achieved for the ETmPoly model (2.8±0.3 K). This model considers all synoptic terms for which there were more than 20 000 RS IWV observations and assumes a fifth-degree polynomial relation between them. More detailed analyses showed that the ETmPoly model performed better during winter (DJF) than summer (JJA) months, which was strongly related to the water vapor variability. The model's impact was also validated against the Bevis model and by comparing the ETmPoly to the conversion of GNSS ZTD to GNSS IWV. The differences obtained between these two approaches reached up to 0.8 mm.

Regional GNSS meteorology studies in Brazil were reported by Mota et al. (2019). The authors evaluated the suitability and performance of the IWV estimates in the state of Rio de Janeiro in Amazonia. This region is characterized by high variability of temperature and relative humidity and high annual rainfall, ranging from about 2000 mm/year in the central part to around 3000 mm/year in its coastal counterpart and in northwestern Amazonia. However, there is a low density of conventional/automatic stations and meteorological radars monitoring weather phenomena. Mota et al. (2019) used one year of GNSS data from the Brazilian Continuous Monitoring Network (RBMC) and the International GNSS Monitoring and Assessment System (iGMAS) in Brazil to estimate GNSS IWV. GNSS estimates were analyzed and compared to retrievals from radiosonde and Moderate Resolution Imaging Spectroradiometer (MODIS). The research showed important differences in the spatiotemporal distribution of water vapor determined by the GNSS-, MODIS-, and radiosonde-derived IWV datasets. This work also confirmed a need to complete the GNSS network in Rio de Janeiro with the meteorological stations near each GNSS receiver. It is intended to improve local IWV estimates and serve as additional support for operational numerical assimilation, weather forecasting, and nowcasting of extreme rainfall and flooding events.

Another study, employing number of GNSS processing technique, considered one of the valleys in Switzerland (Wilgan and Geiger, 2019). This study presents high-resolution models of tropospheric total refractivity and ZTDs for the challenging alpine area of Matter Valley in Switzerland. It is important to provide reliable measurements in the high mountains for monitoring avalanches, deformations, rock glacier activity, or landslides. Here, the authors presented the models based on the numerical weather prediction model COSMO-1 with a high spatial resolution of 1.1 km per 1.1 km, GNSS data from permanent geodetic stations, and GPS L1-only data from low-cost permanent stations. The tropospheric parameters were interpolated to the arbitrary locations by the least-squares collocation method using the software package COMEDIE (Collocation of Meteorological Data for Interpretation and Estimation of Tropospheric Pathdelays). The authors validated generated models against reference radiosonde measurements for total refractivity and GNSS data for ZTD. The accuracy of both GNSS- and NWP-based models was much higher than in previously reported studies e.g., by Wilgan et al. (2017).

This study used a denser GNSS network and NWP model of higher resolution. Thus, the authors concluded that high-resolution input data enhanced the overall accuracy of the tropospheric models.

3.6. GNSS troposphere in numerical weather systems and nowcasting applications efforts

Several studies will take a step further from analyzing severe weather signatures in GNSS signals. These studies demonstrate the application of GNSS observations directly in the weather model assimilation system. Researchers are currently looking into assimilating ZTDs, PWVs, and tomography refractivities.

Rohm et al. (2019) presented the results of assimilating GNSS data into the Weather Research and Forecasting (WRF) NWP model using the WRF data assimilation (WRFDA) package. Two variational approaches, 3DVAR and 4DVAR, were used, and the assimilation procedure was modified to correct bias and observation errors. The assimilated GNSS data included ZTD, PWV, radiosonde (RS), and surface synoptic observations (SYNOP) using a 4DVAR assimilation scheme. Three experiments were conducted to analyze the impact of GNSS data assimilation on weather forecasting, including severe weather events in June 2013. The study revealed that GNSS data assimilation using the GPSPW operator significantly improved the moisture fields and rain forecasts in the WRF model. The strongest impact was observed after a 9-hour lead time. The assimilation of ZTD significantly reduced the mean error of relative humidity forecasts in a vertical profile by over 20%, starting from 2.5 km upward. Assimilation of PWV alone did not significantly improve, but the combination of PW, SYNOP, and radiosonde improved humidity distribution in the vertical profile by up to 12%. In all three analyzed severe weather cases, PWV improved the rain forecast, while ZTD reduced the humidity field bias. Binary rain analysis showed that GNSS parameters significantly impacted the rain forecast in the class above 1 mm/h. Overall, the results suggest that assimilating GNSS data into the WRF model can significantly improve the accuracy of weather forecasting, particularly in moisture fields and rain forecasts.

Another study, led by researchers from the Australian Bureau of Meteorology (Le Marshall et al., 2019), presented the application of the ZTD data provided by GNSS missions in NWP to enhance moisture specification of the atmosphere at up to nearly 40 km resolution across south-eastern Australia. These observations have an accuracy (often equivalent to 2-mm RMS error in total water vapor), which enables them to be of potential benefit for the NWP model and to be of value in the Australian region, which is in the data sparse southern hemisphere. Here the authors used ZTD, produced in real-time/near real-time by RMIT University and Geoscience Australia. It resulted in an enhanced database for the specification of moisture fields in the ACCESS C3 NWP system. The improved database resulted in improvements to 12- and 18-h rainfall forecasts which were measured using the Fractions Skill Score.

Other studies are looking into the innovative use of GNSS tomography refractivity profiles as an input to the NWP data assimilation system. Trzcina and Rohm (2019) es-

tablished an NRT GNSS troposphere tomographic solution for the area of Poland, using TOMO2 software developed at UPWr. The solution is based on the ZTD estimates for 167 GNSS stations from the EUREF Permanent Network, ASG-EUPOS, and Leica SmartNet networks. 3-dimensional reconstruction of the wet refractivity field in the troposphere up to 12 km altitude is provided every 1 hour, using tomographic principles. The NRT experiment and assimilation into the numerical weather prediction (NWP) model were performed to verify whether tomographic products can attain the required accuracy for utilization within operational NWP procedures. The assimilation of the TOMO2 output into a WRF model was performed using the WRF Data Assimilation (WRFDA) module and a GPSREF observation operator dedicated to radio occultation (RO) total refractivity data. Two selected analysis periods covered summer storms and autumn rainfalls. The resulting weather forecasts were validated with GNSS-derived IWV data, synoptic observations, radiosonde profiles, and ERA-Interim reanalysis. The analysis revealed the capability of the TOMO2 model outputs to improve 6–18 hours predictions of relative humidity (0.5%) and temperature (0.25°C), especially for precipitation events.

Hanna et al., (2019) performed the first test on the assimilation of the GNSS tomography products to the Weather Research and Forecasting Data Assimilation System (WRF DA). The tomographic domain covered the area of central Europe. The wet refractivity fields were estimated using two tomographic models (TUW and UPWr) during heavy-precipitation events (May 29 – June, 14, 2013). The authors tested three sets of GNSS slant wet delays (SWDs) derived from ZTDs and horizontal gradients provided for 88 GNSS sites by Geodetic Observatory Pecny (GOP). The analyzed datasets consisted of 'set0' without compensation for hydrostatic anisotropic effects, 'set1' with compensation for this effect, and 'set2' cleaned by wet delays outside the inner voxel model. To perform the three-dimensional assimilation of the GNSS tomography products into the nested (12 km and 36 km horizontal resolution) WRF model, the authors used the radio occultation (GPSREF) observation operator. This operator enabled the assimilation of the total refractivity profiles; therefore, besides the tomographic wet refractivity field, the missing hydrostatic part of refractivity was derived from the ALADIN-CZ model. Moreover, the authors compared GNSS tomography data assimilation results to the radiosonde (RS) observations. The validation showed that the assimilation improved the relative humidity forecasts (bias and standard deviation) and temperature (standard deviation) during heavy-precipitation events.

Prior studies on the assimilation of numerical weather prediction models have utilized observation operators not optimized for GNSS tomography data. Trzcina et al. (2020) introduced TOMOREF, an observation operator designed to assimilate 3-D fields of wet refractivity derived from GNSS tomography data into a WRF DA system. TOMOREF was tested using wet refractivity fields obtained during a heavy precipitation event and validated using radiosonde observations, synoptic data, ERA5 reanalysis, and rain radar data. The results showed that assimilating GNSS tomography data positively impacted the forecast of relative humidity, with a reduction in root-mean-square error of up to 0.5%. Furthermore, the assimilation of GNSS tomography data improved precipitation forecasts within 1 hour after assimilation, as evidenced by a reduction in mean bias values

of up to 0.1 mm. The results also demonstrated that GNSS tomography data had a greater impact on the WRF model than ZTDs, underscoring the potential of GNSS tomography data for weather forecasting.

Finally, the nowcasting of severe weather events using a machine learning approach with GNSS ground-based and tomography retrievals was investigated by Los et al. (2020). The author focused on applying GNSS observations in nowcasting severe weather events, particularly summer storms, which can result in significant economic and societal losses. While previous studies have explored vertical IWV in weather nowcasting, the combination of IWV and vertical profiles of wet refractivity derived from GNSS tomography has not yet been fully utilized for short-range forecasts of storms. The study presented a machine learning approach to predict storms in Poland within a 0–2 hour window using the combined information of IWV and tomography-based vertical profiles. The model was found to be accurate, with a success rate exceeding 87%. However, the precision of the prediction was limited to about 30%. The wet refractivity below 6 km and IWV on the west side of the storm were identified as significant parameters with the potential to predict the location of the storm. Furthermore, the analysis of IWV highlighted a correlation between changes in IWV and the occurrence of storms.

4. Ionosphere studies with GNSS

GNSS-based ionosphere sounding has always played a prominent role in the studies undertaken by the Polish scientific community. In this regard, the investigations are conducted toward ionospheric disturbance monitoring, regional and global ionosphere modeling, and enhancing the algorithms for mitigating ionosphere-originated errors in precise GNSS positioning.

The investigations aimed at high-latitude ionosphere monitoring were conducted at UWM. To provide a more detailed view of plasma irregularities, the authors employed two parameters, namely ROTI and relative STEC (Sieradzki and Paziewski, 2019). The latter is a new approach that extracts signatures of large-scale ionospheric structures by estimating background STEC level with a 4-order polynomial. The main benefit of relative STEC value is its epoch-wise character without spatiotemporal interpolation. More importantly, the indicator can be easily extracted for entire GNSS networks, providing a more comprehensive view of the ionosphere. The comparison of statistics offered by ROTI and relative STEC demonstrated that the new algorithm is especially effective for massive plasma structures. As a consequence of these promising results, the new algorithm was applied to the first climatological study of polar patches using ground-based GNSS observables (Sieradzki and Paziewski, 2022). These investigations revealed the equinoctial peak of polar patch occurrence and a good agreement between GNSS and SWARM measurements. A sparse divergence between both techniques was related to a different patch definition. The analysis also reported a transformation of the UT pattern depending on the ionospheric gradient between sub-auroral and polar areas. During the winter solstice, most patches occurred at post-

noon UT hours, whereas in March, the maximum corresponded to morning hours. This variation was expected according to the theory, but it was confirmed for the first time.

The climatology of ionospheric irregularities over Greenland was, in turn, investigated in the ESA-founded project "Forecasting Space Weather Impacts on Navigation Systems in the Arctic" (FORSWAR). The consortium of UWM, Universitat Politecnica de Catalunya (UPC), University in Oslo (UiO), and German Aerospace Center (DLR) studied modeling and reconstruction of ionospheric irregularities expressed in terms of ROTI by the method of Empirical Orthogonal Functions (EOFs) (Jin et al., 2022). The applied method using ROTI as an input presented the long-term climatology (over two solar cycles) of TEC irregularities from a polar cap station. The climatology revealed variability with different time scales, i.e., solar cycle, seasonal, and diurnal variations. The FORSWAR project also provided a method based on the optical flow algorithm for forecasting ROTI (OFROTI) (Monte-Moreno et al., 2021). It is a nonparametric method for predicting maps of rapid polar ROTI fluctuations. This prediction method involves modeling the ROTI spatial distribution as a time-evolving flow. The method works well in high/medium geomagnetic activity conditions, assuming that the regions of high ROTI values are concentrated with continuity.

The problem of precise positioning under such disturbed ionospheric conditions at high latitudes was investigated in Paziewski et al. (2022). Specifically, the study addressed a research problem regarding the impact of ionospheric irregularities on precise GNSS positioning in Greenland. The authors assessed the performance of positioning methods that had not been comprehensively investigated but are desired by a wide range of users, namely single-frequency (SF) PPP and wide-area RTK. The datasets were acquired under three ionospheric storms: the St. Patrick's Day storm of March 17, 2015, the storm on June 22, 2015, and August 25–26, 2018, to provide a challenging scenario for experimentation. As expected, the results demonstrated noticeable implications of the ionospheric disturbances for the IAR performance and the coordinate accuracy in RTK positioning. More importantly, the authors revealed that the SF PPP model based on the GRAPHIC phase-code ionospheric free linear combination was generally resistant to ionospheric disturbances.

The UWM research group also contributed to developing the global ionosphere models. A new global ionosphere model was proposed based on processing undifferenced dual-frequency GPS+GLONASS carrier phase data from 260 permanent stations and several interpolation techniques. The employed approach is based on a three-step procedure and allows estimating the slant ionospheric delays. These values are derived using the geometry-free linear combination and carrier phase bias modeling. Then, VTEC values are converted into STEC at the ionospheric pierce points (IPP) locations. For this purpose, a Modified Single Layer Model (MSLM) mapping function was used. The application of different stochastic parametric modeling methods to interpolating TEC data in producing this global ionosphere model has been comprehensively examined. The theoretical background related to the parametrization of least-squares collocation (LSC) was studied in parallel with the other techniques from the kriging family, i.e., ordinary kriging (OKR) and universal kriging (UKR) (Jarmolowski et al., 2021b). The studies on the local

ionosphere model in southeastern Asia proved similar accuracy derived from different parametric modeling techniques (Jarmolowski, 2019; Jarmolowski et al., 2019). Special attention was paid to the parametrization and detrending problems related to kriging and LSC. More precisely, it was found that local detrending with higher-order polynomial surfaces applied in UKR adversely affects the kriging modeling results. Additionally, it was concluded that outliers occurrence also decreases kriging accuracy, especially in the case of local, higher-order detrending in UKR (Fig. 8).
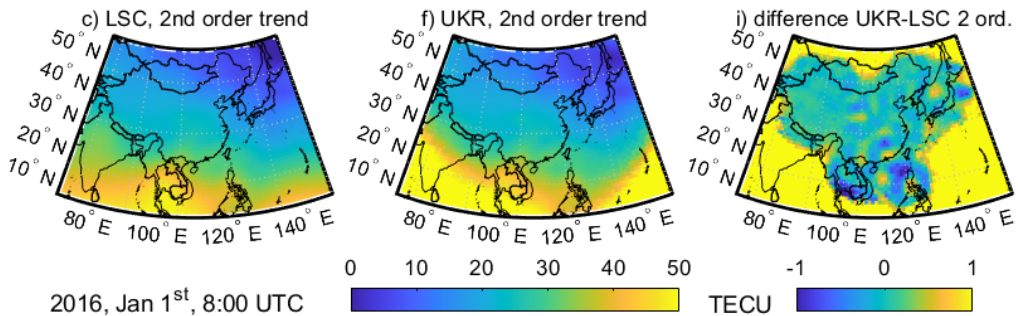
Fig. 8. Example epoch (January 1, 2016, 8:00 AM) of VTEC interpolated by LSC and UKR methods and differences between LSC and kriging for data with outliers

Kriging modeling was recently implemented in the new GIM by UWM. The global grid based on point VTEC data at IPPs was created by combining two kriging techniques in two modeling steps: ordinary kriging (OKR) and simple kriging (SKR) equivalent to LSC (Jarmolowski et al., 2021b). The combination of OKR and SKR was justified mainly by the inhomogeneous geostatistical distribution of TEC point data due to equatorial ionization anomaly (EIA). It required the removal of the long-wavelength VTEC part to ensure work with a relatively homogeneous residual signal in the second step of precise modeling by SKR. The removal of the trend by OKR was an alternative to spherical harmonic detrending, which was more stable in the presence of significant data gaps over the ocean. The second step of precise residual modeling by SKR technique is based on VTEC residuals, which have a substantial advantage with respect to non-detrended VTEC due to an approximate geostatistical homogeneity of residual TEC signal after the elimination of EIA, and due to the narrow band of the processed signal. As a result, the final UWM GIMs are of 2.5 by 5.0 degrees spatial and 1-hour temporal resolution. The accuracy of the new ionosphere model by UWM under various geomagnetic conditions was verified by comparing it to the best available GIMs (Fig. 9). The models were analyzed for self-consistency during the most severe geomagnetic storm of 2018. RMS for UWM GIMs reached the lowest values among all tested models for the stormy day. In general, UWM maps offer a clear improvement over benchmark models provided by IGS and CODE (Wielgosz et al., 2021).
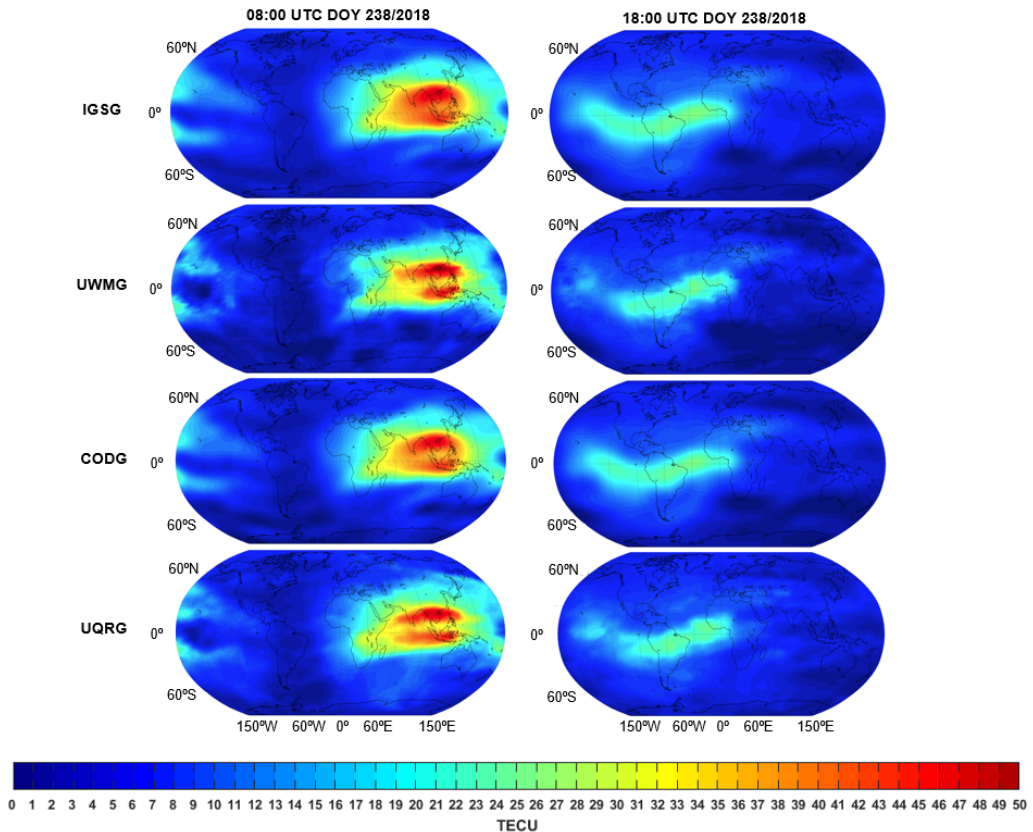
Fig. 9. Example TEC maps derived from IGSG, UWMG, CODG, and UQRG models on a stormy day
(DOY 238) at 08.00 UTC (left) and 18.00 UTC (right)

5. Selected GNSS applications

GNSS positioning proved its high applicability and reliability in providing coordinate estimates. Studies stimulating progress in this area have mainly considered enhancing correction, functional and stochastic models, methods for integer ambiguity resolution and validation, and integration of multi-constellation GNSS signals. Consequently, GNSS positioning has been applied to numerous branches of industry and fields of human activity where high accuracy and reliability of the solution are required. These include surveying, mapping, transport, civil engineering, but also other applications such as geography, hydrology, and even tourism (Szombara et al., 2020; Chwedczuk et al., 2022). Moreover, GNSS positioning with smartphones is gaining popularity as it becomes more and more accurate (Koziol and Maciuk, 2020).

In this section, we acknowledge selected studies reporting the achievements of Polish researchers related to the abovementioned selected GNSS applications. We recognize advances in low-cost and Android GNSS, GNSS seismogeodesy, geodynamics, structural health monitoring (SHM), antenna calibration, and satellite clock stability.

5.1. Positioning and applications with smartphones and low-cost GNSS receivers

Recent advances in GNSS hardware inspired the scientific community to put a spotlight on the mass-market GNSS receivers and smartphones equipped with GNSS chipsets and the development of novel processing methods as a potential complement to the high-grade GNSS receivers in geoscience studies. By taking advantage of the ubiquity of such receivers, we may move towards a new era with multiple sensors acquiring multi-constellation and multi-frequency GNSS observations.

GNSS measurements of smart devices have been accessible through Application Programming Interface 24 on Android 7 since 2016, provoking studies in the field. Despite the unprecedented advances in GNSS chipsets embedded in smart devices, we still may list many constraints that hinder their use in the most demanding applications. The issues such as susceptibility to multipath, the inhomogeneous gain pattern, unmodelled lack of phase centers, and linear polarization affect smartphone GNSS antennas. What is more, high noise of observations, unaligned chipset initial phase biases, and other biases destroying the integer and time-constant properties of carrier-phase ambiguities must be addressed (Paziewski, 2020; Iakovidis et al., 2022).

These smartphone GNSS data limitations have spurred an effort by the scientific community to handle them. Initially, attention has been drawn to the quality of GNSS observations derived from smartphones. In Paziewski et al. (2019a), the authors showed the poor quality of the smartphone GNSS phase data. Specifically, the analyses revealed that smartphone GNSS phase measurements are affected by discontinuities, a gradual accumulation of errors, and the duty cycling effect. These phenomena prevent correct IAR and consequently impede the application of smartphone phase measurement to high-precision positioning techniques such as RTK or PPP. Moreover, even if the most recent smartphones acquire observations on multiple frequencies, selected ones are still subject to unwanted effects that must be handled (Paziewski et al., 2021). Careful addressing of such constraints may catalyze an expansion of satellite navigation to novel science and market areas.

Considering such restrictions, an effort has been put into developing stochastic and functional models customized to smartphone observations. These algorithms aimed to address such limitations of smartphone observations as the low suppression to multipath, high observational noise, the carrier phase discontinuity driven by duty-cycle, and the existence of unwanted biases that destroy integer properties of phase ambiguities. In Paziewski et al. (2019a), the authors suggested the application of wide-range DGNSS positioning to address the constraints of smartphone phase GNSS data. The following studies enhanced weighting schemes by introducing a novel one based on carrier-to-noise density ratio, thus suited for smartphone GNSS data (Robustelli et al., 2021). More importantly, the feasibility of collaborative smartphone-to-smartphone GNSS RTK positioning with IAR has been shown for the first time (Paziewski et al., 2021). In parallel, studies have been conducted on applying low-cost GNSS receivers to geodetic applications. First, a focus has been put on evaluating SDR low-cost receivers' observation quality and positioning performance (Robustelli et al., 2022).

Next, the investigations explored the potential of low-cost receivers and antennas for surveying applications. In Wielgocka et al. (2021), the authors employed the u-blox ZED-F9P receiver and the low-cost ANN-MB-00-00 antenna for assessing PPP, RTK, and relative static positioning performance. The results revealed that the ambiguity fixing rate might reach up to 80% in the static mode, thus providing a few centimeters of horizontal accuracy. A comparable level of accuracy is offered in RTK and Network RTK or PPP mode after at least 2.5 h of data collection. However, a noticeable deterioration was reported when a low-cost receiver was used as a base station for RTK positioning.

Finally, the current performance of single-frequency PPP with low-cost receivers has been evaluated in Paziewski (2022). The author showed the most prominent constraint of such receivers and antennas, which is multipath, and demonstrated the benefit of applying a phase-code ionosphere-free linear combination to low-cost receiver GNSS data processing. Moreover, a great advantage of geodetic antennas over low-cost ones was revealed.

The quality of tropospheric estimates obtained from low-cost equipment was investigated to discuss their suitability for climate and weather applications (Stepniak and Paziewski, 2022). The experiment was based on GNSS data collected during two campaigns in diverse atmospheric conditions. Three collocated stations equipped with u-blox ZED F9P receivers and one station with a high-grade Trimble Alloy receiver were employed for data acquisition. Receivers were connected to two different types of GNSS antennas: a surveying-grade Leica AR10 and a patch ANN-MB antenna. Zenith tropospheric delays and horizontal gradients restored from GNSS data of mass-market receivers were validated against those of the high-grade receivers and the fifth-generation reanalysis for the global climate and weather – ERA5. The results showed that tropospheric parameters derived from low-cost receiver data could achieve high precision and reliability, only slightly lower than that of high-grade receivers. The accuracy of low-cost receiver tropospheric estimates can be better when a surveying-grade antenna is employed than the low-cost receiver + a patch antenna. A strong correspondence between GNSS-derived tropospheric parameters and these of the reanalysis was also revealed. Such an outcome proved that low-cost equipment might contribute to atmospheric studies by taking advantage of their low cost and thus ease of GNSS permanent network densification, increasing the spatial resolution of the soundings.

5.2. GNSS for geohazard and structural health monitoring

High-sampling rate of observations offered by geodetic GNSS receivers opened the door for this measurement technique to seismic, geohazard, and structural health monitoring studies. Such an application of navigation satellite systems is labeled as GPS seismology. The following research considered the determination of subsidence and seismic deformations caused by earthquakes, volcanoes, tsunamis, GPS-based systems for early warnings, and SHM systems. These investigations involved precise positioning techniques or dedicated processing algorithms directly retrieving displacements suited to the GNSS observations of high-grade receivers (Paziewski et al., 2018).

Also, the Polish scientific community has recently contributed to developing and assessing the novel GNSS processing algorithms retrieving dynamic displacements. First, in Paziewski et al. (2019b), the authors presented and validated an enhanced PPP-based approach for characterizing structural vibrations. Taking advantage of artificially triggered high-rate and low-scale vibrations, the authors proved that retrieving the amplitude of such sin-wave displacements at a millimeter-level accuracy is possible. Moreover, with the presented method, it is feasible to process observations even at a 100 Hz rate, which allows for meeting the specific demands of structural displacement monitoring.

Furthermore, in Paziewski et al. (2020), the authors introduced an automatic system for Galileo + GPS high-rate data processing, which addresses the specific requirements of local seismic events monitoring. The system retrieves the displacement response to seismic events induced by mining exploitation based on medium-baseline multi-station positioning algorithms. The results proved that it is possible to offer millimeter-level accuracy of such derived displacements.

The following studies in the field investigated three strong natural earthquakes with HR-GNSS. In Kudlacik (2019) the authors demonstrated the necessity of filtering the HR-GNSS displacement time series to resolve the reliable GNSS-waveforms comparable with seismic waveforms and the suitable filtering methodology that does not require additional reference HR-GNSS data. The presented procedure of denoising the HR-GNSS time series was then adopted into a small and shallow anthropogenic tremor of magnitude 3.7 in south-western Poland in Legnica-Glogow Copper District. This unique study revealed that with the HR-GNSS (limited to GPS), after a proper denoising procedure, small-amplitude vibrations induced by mining activity are reliably recognized compared to seismic sensors. The peak value of ground displacement was 2–14 mm, and the correlation coefficients between GPS and seismological displacement time series reached 0.92 (Kudlacik et al., 2021). These results were also confirmed by Ilieva et al. (2020). Figure 10 depicts the seismometer (SM) results overlayed by the GNSS displacements and the Pearson correlation coefficients showing the best agreement of SM and GNSS time series during the most significant displacements.

Next, the studies explored the idea of applying multi-source satellite observations to the atmosphere and geohazard monitoring. UWM in Olsztyn was the Prime Contractor of the COSTO project (Contribution Of Swarm data to the prompt detection of Tsunamis and Other natural hazards), which also involved the National Observatory of Athens (NOA), Technical University of Munich (TUM/DGFI-TUM) and Technical University of Catalonia (UPC/UPC-IonSAT). The project objective was to characterize and understand coupling processes and interactions between the ionosphere/magnetosphere, the lower atmosphere, and the Earth's surface and sea level vertical displacements. For this purpose, the observations from the Swarm mission, GNSS, and seismic records were combined with information on earthquakes and tsunamis. Specifically, a relationship between seismic ionospheric disturbances and the earthquakes and tsunamis observed from low-Earth-orbit (LEO) satellites was investigated. This research was based on two Swarm data types: in-situ electron density (ED) measured by Langmuir Probes (LP) and total electron content (TEC) from precise orbit determination (POD) GNSS receivers (Jarmolowski et al., 2021a). The mathematical tools applied in this kind of research
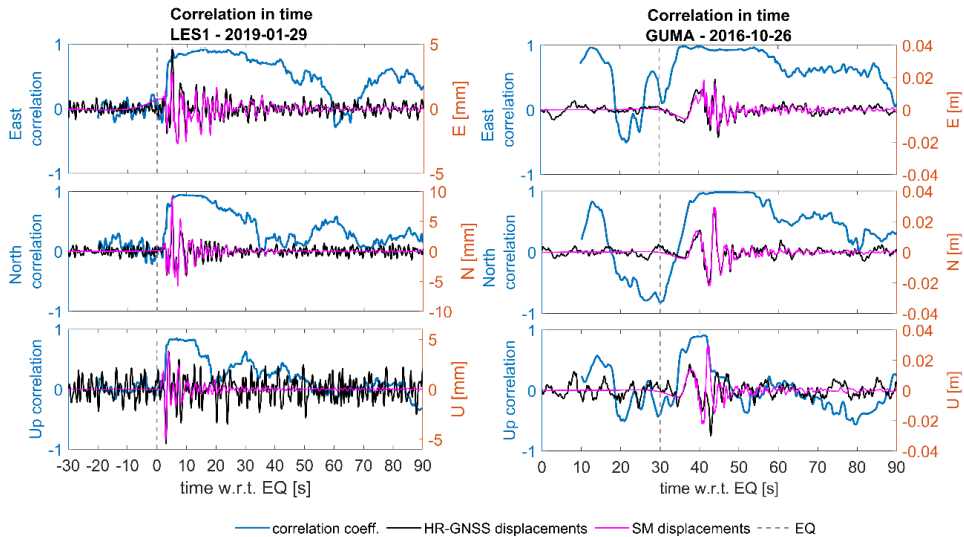
Fig. 10. Pearson's correlation coefficient change in time for mining-induced-tremor (left) and natural earthquake (right). The correlation between SM and GNSS displacements is the highest for the greatest peaks

were Fast Fourier Transform (FFT)-based high-pass and band-pass filters, and short-term Fourier transform (STFT) analysis of seismic ionospheric disturbances (SID) in along-track satellite data. Swarm data processed using STFT was applied in detecting and preliminary classifying SIDs related to earthquakes and tsunamis. In contrast, ground GNSS data and seismic records were engaged in their validation. The analyses of Swarm data provided interesting observations of ionospheric disturbances not only directly related to the most significant earthquake events and tsunamis but also occurred during entire periods of enhanced seismic activity and at larger distances from the earthquake epicenter. The largest earthquake and tsunami examined using Swarm mission data was the Chilean Mw =8.3 earthquake. This event occurred on September 16th, 2015, on the coast of central Chile, near Illapel (Fig. 11). The seismic activity before and after the mainshock-induced SIDs were detected with Swarm and ground GNSS stations (Jarmolowski et al., 2021a). Different ionospheric anomalies were recorded along Swarm satellite orbits located over earthquake/tsunami events at the time of these events or close to them in time and space when a related seismic activity took place. Filtered disturbing signals from Swarm and ground GNSS, observed in the same place and time, were analyzed together. STFT spectrograms were made for the selected Swarm along-track data samples and determined their spectral patterns. Keograms and scatter plotting for ground GNSS carrier phase geometry-free combination data (L_{GF}) from dense ground networks were used for the validation by the analysis of SID's spatiotemporal correlation (Fig. 11). STFT spectral approach to along-track Swarm data studied in the frame COSTO allowed distinguishing the signals of different origins.

The COSTO studies opened a way to analyze the system of seismically induced ionosphere anomalies for a wider range, also including internal validation of the observed
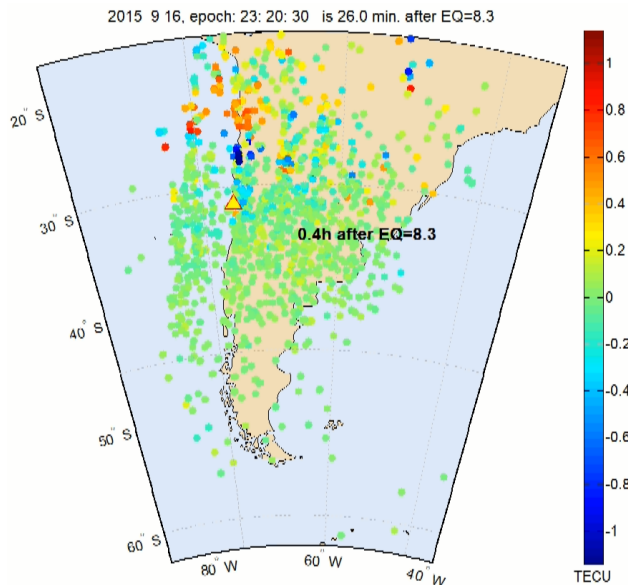
Fig. 11. Scatter map of detrended L_{GF} phase combination from ground GNSS stations of Chilean and Argentinian networks 0.4 h after 8.3 earthquake. The red/blue points in the vicinity of the earthquake denote SIDs, which move to the northeast

anomalous signals. The research outcomes can constitute a basis of a prototype solution for investigating solid Earth-atmosphere-ionosphere coupling.

Extensive studies on applying LEO satellites such as Swarm, GRACE, COSMIC, and DORIS were continued at UWM. Interesting findings referred to the analyses of Swarm electron density (ED) and topside total electron content (TEC) data. The studies focused on the period of increased seismic activity in Papua New Guinea (PNG) and Solomon Islands in December 2016, including two major earthquakes with Mw = 7.8 and 7.9 (Yang et al., 2022). The analyses of Swarm data in the PNG region were based on high-pass filtered ED and POD GNSS TEC time series along the satellite tracks. The STFT and windowing using Tukey window were applied to provide spectrograms of ED and topside TEC over seismically active tectonic plate boundaries, over which the Swarm passes were recorded. Figure 12 presents an example spectrogram of a selected interesting Swarm passes over the PNG region recorded around 40 min after the second major earthquake with Mw = 7.9 in PNG. The ED residual signal revealed significant power spectral density (PSD) values at different separated spectral periods, which is suspected to be characteristic for the ionosphere responses to sudden seismic activity detectable by LEO satellites. The observations of residual Swarm ED signal suggested that maximum PSD variations of Swarm ED are correlated with seismic activity starting from 5.0 magnitude in the region of two analyzed mainshocks. It can be observed that the most prominent peaks of ED PSD maxima at different periods occur with critical seismic activity, like the first earthquake after relaxation, a larger earthquake amongst some number of smaller earthquakes, or the largest earthquakes in the region. The lowest PSD of ED typically

coincides with relaxation time. Swarm ED disturbances have specific spectral patterns in different moments of continuous tectonic activity. Therefore, these studies suggested that continuous tracking of seismic activity from the satellite orbit is fundamental in LEO-based seismology and can provide inputs to the research on earthquake forecasting. The validation of spectral analysis has been made to compare disturbed in-situ ED signal and topside TEC signal disturbed by the same seismic events. It should be pointed out that these two kinds of signals refer to geometrically different spatial locations. Therefore an approximate similarity could be only expected, rather than absolute coherency of the signals. Nevertheless, the similarity between ED and POD TEC was very high. The coincidence of PSD from LPs and GNSS TEC confirmed the ionospheric origin of the disturbances and excluded instrumental uncertainties.
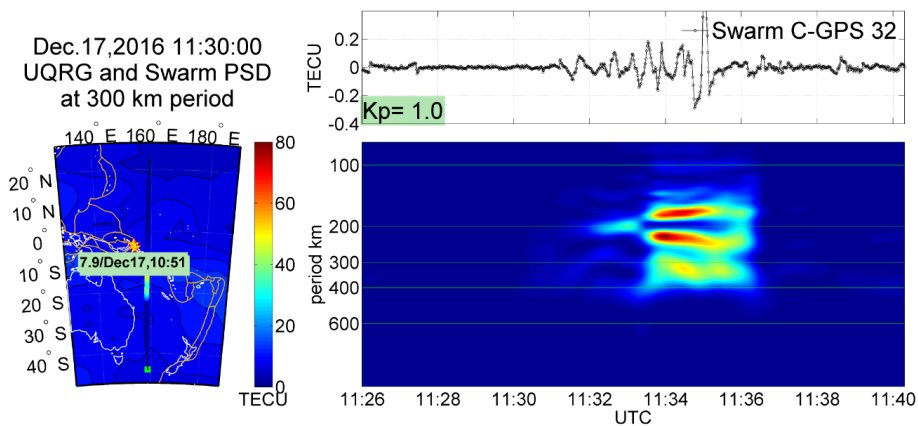
Fig. 12. STFT spectrogram of residual TEC from Swarm C POD GNSS receiver (phase measurements to PRN32) on December 17, 2016, around 40 min after major earthquake with Mw = 7.9

5.3. GNSS antenna calibrations and the stability of satellite clocks

Introducing new carrier frequencies to the mature and developing GNSS systems requires updating the receiver antenna calibration models. Even now, most high-grade GNSS receivers acquire multi-constellation and multi-frequency signals. Therefore, all the geodetic antennas must be calibrated for the new signals shortly. In Krzan et al. (2020), the authors analyzed the differences between phase center corrections (PCC) models of GNSS antennas obtained from field calibration and calibration performed in an anechoic chamber. They also examined the effect of using different PCC models on the EUREF Permanent GNSS Network (EPN) station position time series. The results showed that the calibration method has a noticeable effect on the PCC models. PCC differences determined for ionospheric-free linear combinations can reach up to 20 mm for some antenna signal reception areas, which directly propagates to the coordinate domain. Tests have shown that the differences in height components resulting from different PCC models can exceed 10 mm in some processing variants.

Other symptoms of GNSS modernization are the changes in equipment at reference stations. Hardware changes often cause jumps seen in the time series of station positions. The resulting shifts are assumed to be driven primarily by changes in carrier phase multipath effects after antenna replacement. However, the observed position shifts may also indicate an imperfect in antenna PCC models. In Dawidowicz et al. (2023), the authors analyzed coordinate changes caused by antenna replacement at selected stations of the EPN network. The authors studied the correlation between the occurrence of jumps and the type of PCC model (type mean (IGS), individual robot-derived (ROBOT), individual chamber-derived (CHAMBER)), as well as multipath changes after antenna replacement. The results proved that antenna change is a critical moment in station coordinate stability. In most cases, it causes visible shifts in the time series of position components (Fig. 13). The discontinuities resulting from antenna changes were noted in the position time series in 75% of GPS+Galileo solutions. In contrast, multipath changes resulting from antenna replacement were responsible for 21%–42% of the jumps in the position components depending on the type of solution.
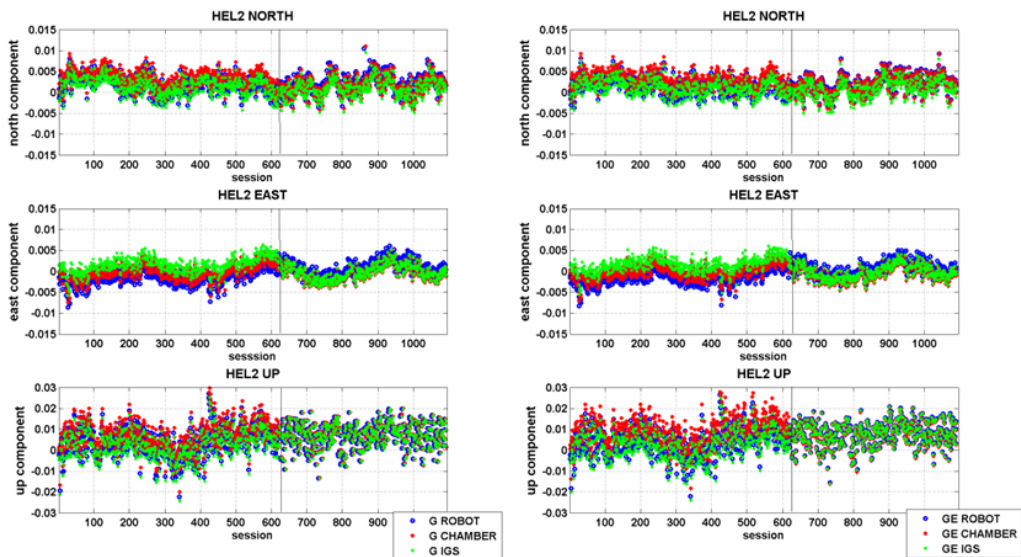
Fig. 13. Time series of NEU position components differences for HEL2 station using different PCC models in case of G-only (G) and GPS+Galileo (GE) observations processing (vertical line indicates the moment of antenna replacement on the station)

In 2019, the consortium of the UWM in Olsztyn and Astri Poland started an ESA-founded project to develop and implement a calibration procedure for multi-frequency and multi-GNSS. The concept of absolute field calibration inspired the methodology used in the project; however, some innovations were introduced (Fig. 14). The first test results proved the correctness of the implemented calibration procedures (Dawidowicz et al., 2021). The calibration results for the L1 GPS frequency showed good agreement with the values included in the IGS-type mean models. For signals from satellites on high

elevations (20° − 90°), the differences did not exceed 1.5 mm. For low elevation angles (0°–20°), the agreement of the results was slightly worse, with differences exceeding the 3 mm level in some cases.

Fig. 14. The test GNSS receiver antenna calibration facility at UWM Olsztyn

Also, MUT in Warsaw reported worth acknowledging findings on the effect of the antenna phase center modeling (Araszkiewicz et al., 2019). The analysis compared IGS-type models and individual calibrations collected by EUREF Permanent GNSS Network (EPN) Central Bureau. The research was conducted using the example of the most popular antenna in the EPN installed in 2015 – Leica's model AR25 with LEIT radome (IGS code: LEIAR25.R3 LEIT). The analyses focused on the estimated heights, as previous investigations showed that this component is most affected by antenna modeling. The analysis of GPS observations of a full year from selected EPN stations revealed that the coordinate solutions are close regardless of the chosen phase center model. The study also demonstrated a relationship between the distribution of differences in the compared phase center correction and the differences in the estimated heights. At the same time, it has been proved that IGS-type mean models provide the same quality of coordinate time series as individual ones. In the following years, the MUT also analyzed how the estimated coordinates were affected by the interchangeable use of phase center corrections intended for the L2 frequency to the E5a frequency (Araszkiewicz and Kiliszek, 2020). Tests were conducted to model the phase position of the antennas in different ways so that the magnitude of the introduced error could be determined. The results demonstrated that using L2 corrections for the E5a frequency introduces a systematic error close to 8 mm. Such simplification applies to nearly half of the EPN stations acquiring Galileo observation at that time.

Furthermore, Borowski et al. (2022) noticed significant inconsistencies in the antenna PCC model between the IGS model and actual antenna characteristics. They used two co-located stations, i.e., KRAW equipped with ASH70195C_M SNOW antenna, which originated from the '90s, and KRA1, having individual calibration provided in 2019.

Various experiments were performed using several calculation strategies, software, and PCC models. The benchmark difference of heights between antennas ARP's points was defined by precise spirit leveling. Surprisingly, the PPP methods performed by network solution or calculated in Bernese Software obtained worse results than those in popular engineering software, such as Trimble Business Centre, GNSS Solutions, or Geonet 2006 (Fig. 15). Authors emphasized that the stations included in CORS networks need individual antenna calibration, and the antennas from the '90s should be replaced by new ones supporting all constellations.
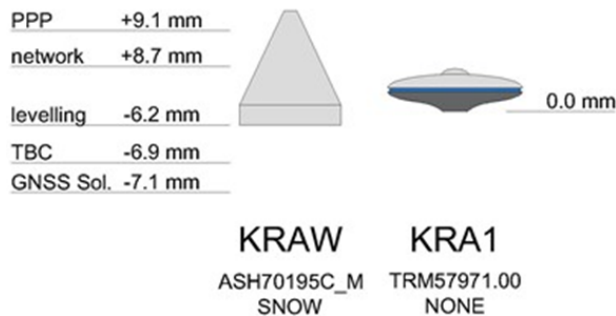
Fig. 15. The height difference between the antenna reference points (ARP) defined by different methods (PPP – PPP calculated in Bernese, network – EPN weekly solutions, TBC – Trimble Business Centre 3.5, GNSS Sol. – GNSS Solution 3.80.8)

Also, the GNSS satellite onboard clocks were of interest to Polish researchers. Maciuk et al. (2021) analyzed the stability of GPS and Galileo onboard oscillators. At the same time Maciuk (2019a), and Maciuk and Lewinska (2019) carried out GPS clock stability analyses based on the original 1 Hz clock correction product calculated with the Bernese GNSS Software. It was demonstrated that the stability of the hydrogen maser clock is by one order of magnitude and by half order of magnitude better than for the internal and cesium clocks, respectively. In the following studies, Galileo and BeiDou clocks were also taken into consideration. Maciuk (2019b) noticed some events of unexpected and unexplained jumps in Galileo's clock corrections as well as he analyzed anomalous trends and frequency behavior in the clock characteristics. Ai et al. (2021) focused on determining the noise characteristic of the different types of clocks (rubidium, cesium, hydrogen masers), the type of GNSS system, and the duration of satellites in orbit.

6. Summary and conclusions

This review paper acknowledged the most important research activities concerning GNSS positioning and applications conducted at Polish research institutions in the period of 2019–2022. In particular, we discussed the advances in PPP and relative positioning, troposphere, and ionosphere sounding, smartphone and low-cost GNSS data processing, and other specific studies such as those on satellite antenna calibration and clock stability. Still, we recognize numerous emerging and inevitable issues related to, e.g., multi-

constellation signals fusion and biases, which need to be carefully handled. Nonetheless, in light of these recent advances in theories and algorithms, continuous progress in GNSS performance is thought to be maintained in the future, and GNSS applications are expected to continue to proliferate.

We offer special words of thanks to the researchers who contributed to this review with their articles. We anticipate their studies will spark further innovations in geodesy, geomatics, and related applications. We also express our gratitude to the Committee on Geodesy of the Polish Academy of Science, which initiated this review article reporting the recent contribution of the Polish research community to GNSS science.

Author contributions

Conceptualization: J.P., T.H., W.R., P.W.; writing original draft preparation: J.P., T.H., W.R., P.W.; writing – review and editing: J.P., T.H., W.R., P.W.

Data availability statement

No datasets were used in this research.

Acknowledgements

References

Adavi, Z., Rohm, W., and Weber, R. (2020). Analyzing Different Parameterization Methods in GNSS Tomography Using the COST Benchmark Dataset. *IEEE J. Sel. Top. Appl. Earth Obs. Remote Sens.*, 13, 6155–6163. DOI: 10.1109/JSTARS.2020.3027909.

Adavi, Z., Weber, R., and Rohm, W. (2022). Pre-analysis of GNSS tomography solution using the concept of spread of model resolution matrix. *J. Geod.*, 96, 27. DOI: 10.1007/s00190-022-01620-1.

Ai, Q., Maciuk, K., Lewinska, P. et al. (2021). Characteristics of Onefold Clocks of GPS, Galileo, BeiDou and GLONASS Systems. *Sensors*, 21, 2396. DOI: 10.3390/s21072396.

Araszkiewicz, A., Kiliszek, D., and Podkowa, A. (2019). Height Variation Depending on the Source of Antenna Phase Centre Corrections: LEIAR25.R3 Case Study. *Sensors*, 19, 4010. DOI: 10.3390/s19184010.

Araszkiewicz, A., and Kiliszek, D. (2020). Impact of Using GPS L2 Receiver Antenna Corrections for the Galileo E5a Frequency on Position Estimates. *Sensors*, 20, 5536. DOI: 10.3390/s20195536.

Araszkiewicz, A., Kiliszek, D., Mierzwiak, M. et al. (2021). GPS-Based Multi-Temporal Variation in Precipitable Water over the Territory of Poland. *Remote Sens.*, 13, 2960. DOI: 10.3390/rs13152960.

Baldysz, Z., and Nykiel, G. (2019). Improved Empirical Coefficients for Estimating Water Vapor Weighted Mean Temperature over Europe for GNSS Applications. *Remote Sens.*, 11, 1995. DOI: 10.3390/rs11171995.

Baldysz, Z., Nykiel, G., Latos, B. et al. (2021). Interannual Variability of the GNSS Precipitable Water Vapor in the Global Tropics. *Atmosphere*, 12, 1698. DOI: 10.3390/atmos12121698.

Borowski, L., Kudrys, J., Kubicki, B. et al. (2022). Phase Centre Corrections of GNSS Antennas and Their Consistency with ATX Catalogues. *Remote Sens.*, 14, 3226. DOI: 10.3390/rs14133226.

Brenot, H., Rohm, W., Kačmařík, M. et al. (2019). Cross-Comparison and Methodological Improvement in GPS Tomography. *Remote Sens.*, 12, 30. DOI: 10.3390/rs12010030.

Cellmer, S., Nowel, K., and Fischer, A. (2022a). A search step optimization in an ambiguity function-based GNSS precise positioning. *Surv. Rev.*, 54, 117–124. DOI: 10.1080/00396265.2021.1885947.

Cellmer, S., Nowel, K., and Fischer, A. (2022b). Reduction as an improvement of a precise satellite positioning based on an ambiguity function. *J. Appl. Geod.*, 16, 385–392. DOI: 10.1515/jag-2022-0005.

Chwedczuk, K., Cienkosz, D., Apollo, M. et al. (2022). Challenges related to the determination of altitudes of mountain peaks presented on cartographic sources. *Geodetski vestnik*, 66, 49–59. DOI: 10.15292/geodetski-vestnik.2022.01.49-59.

Dawidowicz, K. (2019). Sub-hourly precise point positioning accuracy analysis – case study for selected ASG-EUPOS stations. *Surv. Rev.*, 52, 341–351. DOI: 10.1080/00396265.2019.1579988.

Dawidowicz, K., Rapinski, J., Smieja, M. et al. (2021). Preliminary Results of an Astri/UWM EGNSS Receiver Antenna Calibration Facility. *Sensors*, 21, 4639. DOI: 10.3390/s21144639.

Dawidowicz, K., Krzan, G., and Wielgosz, P., (2023). Offsets in the EPN station position time series resulting from antenna/radome changes: PCC type-dependent model analyses. *GPS Solut.*, 27, 9. DOI: 10.1007/s10291-022-01339-8.

Ejigu, Y.G., Teferle, F.N., Klos, A. et al. (2021). Monitoring and prediction of hurricane tracks using GPS tropospheric products. *GPS Solut.*, 25, 76. DOI: 10.1007/s10291-021-01104-3.

Fischer, A., Cellmer, S., and Nowel, K. (2022). Regularizing ill-posed problem of single-epoch precise GNSS positioning using an iterative procedure. *J. Appl. Geod.*, 16, 247–264. DOI: 10.1515/jag-2021-0031.

Hadas, T., Kazmierski, K., and Sosnica, K. (2019). Performance of Galileo-only dual-frequency absolute positioning using the fully serviceable Galileo constellation. *GPS Solut.*, 23. DOI: 10.1007/s10291-019-0900-9.

Hadas, T., Hobiger, T., and Hordyniec, P. (2020). Considering different recent advancements in GNSS on real-time zenith troposphere estimates. *GPS Solut.*, 24. DOI: 10.1007/s10291-020-01014-w.

Hadas, T., and Hobiger, T. (2021). Benefits of Using Galileo for Real-Time GNSS Meteorology. *IEEE Geosci. Remote Sens. Lett.*, 18, 1756-1760. DOI: 10.1109/LGRS.2020.3007138.

Hadas, T., Bender, M., Marut, G. et al. (2021). Real-Time GNSS Meteorology in Europe – Hurricane Lorenzo Case Study. In: 2021 IEEE International Geoscience and Remote Sensing Symposium IGARSS. Presented at the IGARSS 2021–2021 IEEE International Geoscience and Remote Sensing Symposium, IEEE, Brussels, Belgium, pp. 8321–8323. DOI: 10.1109/IGARSS47720.2021.9554690.

Haji-Aghajany, S., Amerian, Y., Verhagen, S. et al. (2020). An Optimal Troposphere Tomography Technique Using the WRF Model Outputs and Topography of the Area. *Remote Sens.*, 12, 1442. DOI: 10.3390/rs12091442.

Haji-Aghajany, S., Amerian, Y., Verhagen, S. et al. (2021). The effect of function-based and voxel-based tropospheric tomography techniques on the GNSS positioning accuracy. *J. Geod.*, 95, 78. DOI: 10.1007/s00190-021-01528-2.

Hanna, N., Trzcina, E., Möller, G. et al. (2019). Assimilation of GNSS tomography products into the Weather Research and Forecasting model using radio occultation data assimilation operator. *Atmos. Meas. Tech.,* 12, 4829-4848. DOI: 10.5194/amt-12-4829-2019.

Hordyniec, P., Huang, C.-Y., Liu, C.-Y. et al. (2019). GNSS radio occultation profiles in the neutral atmosphere from inversion of excess phase data. *Terr. Atmos. Ocean. Sci.*, 30, DOI: 10.3319/TAO.2018.10.12.01.

Iakovidis, D.K., Ooi, M., Kuang, Y.C. et al. (2022). Roadmap on signal processing for next generation measurement systems. *Meas. Sci. Technol.*, 33, 012002. DOI: 10.1088/1361-6501/ac2dbd.

Ilieva, M., Rudzinski, L., Pawluszek-Filipiak, K. et al. (2020). Combined Study of a Significant Mine Collapse Based on Seismological and Geodetic Data – 29 January 2019, Rudna Mine, Poland. *Remote Sens.*, 12, 1570. DOI: 10.3390/rs12101570.

Jarmolowski, W. (2019). On the relations between signal spectral range and noise variance in least-squares collocation and simple kriging: example of gravity reduced by EGM2008 signal. *BGTA*. DOI: 10.4430/bgta0265.

Jarmolowski, W., Ren, X., Wielgosz, P. et al. (2019). On the advantage of stochastic methods in the modeling of ionospheric total electron content: Southeast Asia case study. *Meas. Sci. Technol*., 30, 044008. DOI: 10.1088/1361-6501/ab0268.

Jarmolowski, W., Belehaki, A., Hernández Pajares, M. et al. (2021a). Combining Swarm Langmuir probe observations, LEO-POD-based and ground-based GNSS receivers and ionosondes for prompt detection of ionospheric earthquake and tsunami signatures: case study of 2015 Chile-Illapel event. *J. Space Weather Space Clim.*, 11, 58. DOI: 10.1051/swsc/2021042.

Jarmolowski, W., Wielgosz, P., Ren, X. et al. (2021b). On the drawback of local detrending in universal kriging in conditions of heterogeneously spaced regional TEC data, low-order trends and outlier occurrences. *J. Geod.*, 95, 2. DOI: 10.1007/s00190-020-01447-8.

Jin, Y., Clausen, L.B.N., Miloch, W.J. et al. (2022). Climatology and Modeling of Ionospheric Irregularities over Greenland Based on Empirical Orthogonal Function Method. *J. Space Weather Space Clim.*, DOI: 10.1051/swsc/2022022.

Kazmierski, K., Hadas, T., and Sosnica, K. (2018). Weighting of Multi-GNSS Observations in Real-Time Precise Point Positioning. *Remote Sens*., 10, 84. DOI: 10.3390/rs10010084.

Kazmierski, K., Zajdel, R., and Sosnica, K. (2020). Evolution of orbit and clock quality for real-time multi-GNSS solutions. *GPS Solut.*, 24. DOI: 10.1007/s10291-020-01026-6.

Kiliszek, D., and Kroszczynski, K. (2020). Performance of the precise point positioning method along with the development of GPS, GLONASS and Galileo systems. *Measurement*, 164, 108009. DOI: 10.1016/j.measurement.2020.108009.

Kiliszek, D., Kroszczynski, K., and Araszkiewicz, A. (2022). Analysis of Different Weighting Functions of Observations for GPS and Galileo Precise Point Positioning Performance. *Remote Sens.*, 14, 2223. DOI: 10.3390/rs14092223.

Koziol, K., and Maciuk, K. (2020). New heights of the highest peaks of Polish mountain ranges. *Remote Sens.*, 12, 1446. DOI: 10.3390/rs12091446.

Krasuski, K., and Wierzbicki, D. (2021). New Methodology for Computing the Aircraft's Position Based on the PPP Method in GPS and GLONASS Systems. *Energies*, 14, 2525. DOI: 10.3390/en14092525.

Krzan, G., Dawidowicz, K., and Wielgosz, P. (2020). Antenna phase center correction differences from robot and chamber calibrations: the case study LEIAR25. *GPS Solut.*, 24, 44. DOI: 10.1007/s10291-020-0957-5.

Kudlacik, I. (2019). Seismic phenomena in tke light high-rate GPS precise point positioning results. *Acta Geodyn. et Geomater.*, 99–112. DOI: 10.13168/AGG.2019.0008.

Kudlacik, I., Kaplon, J., Lizurek, G. et al. (2021). High-rate GPS positioning for tracing anthropogenic seismic activity: The 29 January 2019 mining tremor in Legnica–Glogow Copper District, Poland. *Measurement*, 168, 108396. DOI: 10.1016/j.measurement.2020.108396.

Lasota, E., Rohm, W., Guerova, G. et al. (2020a). A Comparison Between Ray-Traced GFS/WRF/ERA and GNSS Slant Path Delays in Tropical Cyclone Meranti. *IEEE Trans. Geosci. Remote Sens.*, 58, 421–435. DOI: 10.1109/TGRS.2019.2936785.

Lasota, E., Steiner, A.K., Kirchengast, G. et al. (2020b). Tropical cyclones vertical structure from GNSS radio occultation: an archive covering the period 2001-2018. *Earth Syst. Sci. Data*, 12, 2679–2693. DOI: 10.5194/essd-12-2679-2020.

Lasota, E. (2021). Comparison of different machine learning approaches for tropospheric profiling based on COSMIC-2 data. *Earth Planets Space*, 73, 221. DOI: 10.1186/s40623-021-01548-4.

Lasota, E., Slavchev, M., Guerova, G. et al. (2022). Combined Space- and Ground-Based GNSS Monitoring of Two Severe Hailstorm Cases in Bulgaria. *J. Atmos. Ocean. Technol.*, 39, 649–665. DOI: 10.1175/JTECH-D-21-0100.1.

Le Marshall, J., Norman, R., Howard, D. et al. (2019). Using GNSS Data for Real-time Moisture Analysis and Forecasting over the Australian Region I. The System. *JSHESS*, 69, 1–21. DOI: 10.22499/3.6901.009.

Los, M., Smolak, K., Guerova, G. et al. (2020). GNSS-Based Machine Learning Storm Nowcasting. *Remote Sens.*, 12, 2536. DOI: 10.3390/rs12162536.

Maciuk, K. (2019a). Satellite clock stability analysis depending on the reference clock type. *Arab. J. Geosci.*, 12. DOI: 10.1007/s12517-018-4069-2.

Maciuk, K. (2019b). Monitoring of Galileo on-board oscillators variations, disturbances &amp$ \mathsemicolon$ noises. *Measurement*, 147, 106843. DOI: 10.1016/j.measurement.2019. 07.071.

Maciuk, K., and Lewinska, P. (2019). High-Rate Monitoring of Satellite Clocks Using Two Methods of Averaging Time. *Remote Sens.*, 11, 2754. DOI: 10.3390/rs11232754.

Maciuk, K., Kudrys, J., Skorupa, B. et al. (2021). Testing the product quality of Galileo and GPS on-board oscillators. *Measurement*, 167, 108261. DOI: 10.1016/j.measurement.2020.108261.

Marut, G., Hadas, T., Kaplon, J. et al. (2022). Monitoring the Water Vapor Content at High Spatio-Temporal Resolution Using a Network of Low-Cost Multi-GNSS Receivers. *IEEE Trans. Geosci. Remote Sens.*, 60, 1–14. DOI: 10.1109/TGRS.2022.3226631.

Monte-Moreno, E., Hernandez-Pajares, M., Yang, H. et al. (2021). Method for Forecasting Ionospheric Electron Content Fluctuations Based on the Optical Flow Algorithm. *IEEE Trans. Geosci. Remote Sens.,* 60, 1–1. DOI: 10.1109/TGRS.2021.3126888.

Mota, G.V., Song, S., and Stepniak, K. (2019). Assessment of Integrated Water Vapor Estimates from the iGMAS and the Brazilian Network GNSS Ground-Based Receivers in Rio de Janeiro. *Remote Sens.*, 11, 2652. DOI: 10.3390/rs11222652.

Nowel, K., Cellmer, S., and Fischer, A. (2021). Validation of GNSS baseline observation models using information criteria. *Surv. Rev.*, 53, 402–414. DOI: 10.1080/00396265.2020.1790168.

Nykiel, G., Figurski, M., and Baldysz, Z. (2019). Analysis of GNSS sensed precipitable water vapour and tropospheric gradients during the derecho event in Poland of 11th August 2017. *J. Atmos. Sol. Terr. Phys.*, 193, 105082. DOI: 10.1016/j.jastp.2019.105082.

Paziewski, J., Sieradzki, R., and Baryla, R. (2018). Multi-GNSS high-rate RTK, PPP and novel direct phase observation processing method: application to precise dynamic displacement detection. *Meas. Sci. Technol.*, 29, 035002. DOI: 10.1088/1361-6501/aa9ec2.

Paziewski, J., Sieradzki, R., and Baryla, R. (2019a). Signal characterization and assessment of code GNSS positioning with low-power consumption smartphones. *GPS Solut.*, 23, 98. DOI: 10.1007/s10291-019-0892-5.

Paziewski, J., Sieradzki, R., Baryla, R. (2019b). Detection of Structural Vibration with High-Rate Precise Point Positioning: Case Study Results Based on 100 Hz Multi-GNSS Observables and Shake-Table Simulation. *Sensors*, 19, 4832. DOI: 10.3390/s19224832.

Paziewski, J. (2020). Recent advances and perspectives for positioning and applications with smartphone GNSS observations. *Meas. Sci. Technol.*, 31, 091001. DOI: 10.1088/1361-6501/ab8a7d.

Paziewski, J., and Sieradzki, R. (2020a). Enhanced wide-area multi-GNSS RTK and rapid static positioning in the presence of ionospheric disturbances. *Earth Planets Space*, 72, 110. DOI: 10.1186/s40623-020-01238-7.

Paziewski, J., and Sieradzki, R. (2020b). On the performance of selected ionospheric modelling schemes in Precise Point Positioning. In: 2020 International Conference on Localization and GNSS (ICL-GNSS). Presented at the 2020 International Conference on Localization and GNSS (ICL-GNSS), IEEE, Tampere, Finland, pp. 1–5. DOI: 10.1109/ICL-GNSS49876.2020.9115506.

Paziewski, J., Kurpinski, G., Wielgosz, P. et al. (2020). Towards Galileo + GPS seismology: Validation of high-rate GNSS-based system for seismic events characterisation. *Measurement*, 166, 108236. DOI: 10.1016/j.measurement.2020.108236.

Paziewski, J., Fortunato, M., Mazzoni, A. et al. (2021). An analysis of multi-GNSS observations tracked by recent Android smartphones and smartphone-only relative positioning results. *Measurement,* 175, 109162. DOI: 10.1016/j.measurement.2021.109162.

Paziewski, J. (2022). Multi-constellation single-frequency ionospheric-free precise point positioning with low-cost receivers. *GPS Solut.*. 26, 23. DOI: 10.1007/s10291-021-01209-9.

Paziewski, J., Høeg, P., Sieradzki, R. et al. (2022). The implications of ionospheric disturbances for precise GNSS positioning in Greenland. *J. Space Weather Space Clim.*, 12, 33. DOI: 10.1051/swsc/2022029.

Pelc-Mieczkowska, R. (2020). Preliminary Analysis of the Applicability of the GPS PPP Method in Geodynamic Studies. *Geomat. Environ. Eng.*, 14, 57–68. DOI: 10.7494/geom.2020.14.4.57.

Pelc-Mieczkowska, R., and Tomaszewski, D. (2020). Space State Representation Product Evaluation in Satellite Position and Receiver Position Domain. *Sensors*, 20, 3791. DOI: 10.3390/s20133791.

Poniatowski, M., and Nykiel, G. (2020). Degradation of Kinematic PPP of GNSS Stations in Central Europe Caused by Medium-Scale Traveling Ionospheric Disturbances During the St. Patrick's Day 2015 Geomagnetic Storm. *Remote Sens.*, 12, 3582. DOI: 10.3390/rs12213582.

Prochniewicz, D., Szpunar, R., Kozuchowska, J. et al. (2020). Performance of Network-Based GNSS Positioning Services in Poland: A Case Study. *J. Surv. Eng.*, 146, 05020006. DOI: 10.1061/(ASCE)SU.1943-5428.0000316.

Prochniewicz, D., and Grzymala, M. (2021). Analysis of the Impact of Multipath on Galileo System Measurements. *Remote Sens.*, 13, 2295. DOI: 10.3390/rs13122295.

Prochniewicz, D., Wezka, K., and Kozuchowska, J. (2021). Empirical Stochastic Model of Multi-GNSS Measurements. *Sensors*, 21, 4566. DOI: 10.3390/s21134566.

Prochniewicz, D., Kudrys, J., and Maciuk, K. (2022). Noises in Double-Differenced GNSS Observations. *Energies*, 15, 1668. DOI: 10.3390/en15051668.

Robustelli, U., Paziewski, J., and Pugliano, G. (2021). Observation Quality Assessment and Performance of GNSS Standalone Positioning with Code Pseudoranges of Dual-Frequency Android Smartphones. *Sensors*, 21. DOI: 10.3390/s21062125.

Robustelli, U., Cutugno, M., Paziewski, J. et al. (2022). GNSS-SDR pseudorange quality and single point positioning performance assessment. *Appl Geomat.*, DOI: 10.1007/s12518-022-00457-9.

Rohm, W., and Bosy, J. (2009). Local tomography troposphere model over mountains area. *Atmos. Res.*, 93, 777–783. DOI: 10.1016/j.atmosres.2009.03.013.

Rohm, W., Guzikowski, J., Wilgan, K. et al. (2019). 4DVAR assimilation of GNSS zenith path delays and precipitable water into a numerical weather prediction model WRF. *Atmos. Meas. Tech.*, 12, 345–361. DOI: 10.5194/amt-12-345-2019.

Sá, A., Rohm, W., Fernandes, R.M. et al. (2021). Approach to leveraging real-time GNSS tomography usage. *J. Geod.*, 95, 8. DOI: 10.1007/s00190-020-01464-7.

Sieradzki, R., and Paziewski, J. (2019). GNSS-based analysis of high latitude ionospheric response on a sequence of geomagnetic storms performed with ROTI and a new relative STEC indicator. *J. Space Weather Space Clim.*, 9, A5. DOI: 10.1051/swsc/2019001.

Sieradzki, R., and Paziewski, J. (2022). Towards a reliable ionospheric polar patch climatology with ground-based GNSS. *IEEE Trans. Geosci. Remote Sens.*, 60, 1–14. DOI: 10.1109/TGRS.2022.3149635.

Stepniak, K., Bock, O., Bosser, P. et al. (2022). Outliers and uncertainties in GNSS ZTD estimates from double-difference processing and precise point positioning. *GPS Solut.*, 26, 74. DOI: 10.1007/s10291-022-01261-z.

Szombara, S., Lewinska, P., Zadlo, A. et al. (2020). Analyses of the Prądnik riverbed shape based on archival and contemporary data sets – old maps, LiDAR, DTMs, orthophotomaps and cross-sectional profile measurements. *Remote Sens.*, 12, 2208. DOI: 10.3390/rs12142208.

Tondas, D., Kaplon, J., and Rohm, W. (2020). Ultra-fast near real-time estimation of troposphere parameters and coordinates from GPS data. *Measurement*, 162, 107849. DOI: 10.1016/j.measurement.2020.107849.

Trzcina, E., and Rohm, W. (2019). Estimation of 3D wet refractivity by tomography, combining GNSS and NWP data: First results from assimilation of wet refractivity into NWP. *Q.J.R. Meteorol. Soc.*, 145, 1034–1051. DOI: 10.1002/qj.3475.

Trzcina, E., Hanna, N., Kryza, M. et al. (2020). TOMOREF Operator for Assimilation of GNSS Tomography Wet Refractivity Fields in WRF DA System. *J. Geophys. Res. Atmos.*, 125. DOI: 10.1029/2020JD032451.

Van Malderen, R., Pottiaux, E., Klos, A. et al. (2020). Homogenizing GPS Integrated Water Vapor Time Series: Benchmarking Break Detection Methods on Synthetic Data Sets. *Earth Space Sci.,* 7. DOI: 10.1029/2020EA001121.

Wielgocka, N., Hadas, T., Kaczmarek, A. et al. (2021). Feasibility of Using Low-Cost Dual-Frequency GNSS Receivers for Land Surveying. *Sensors*, 21, 1956. DOI: 10.3390/s21061956.

Wielgosz, P., Milanowska, B., Krypiak-Gregorczyk, A. et al. (2021). Validation of GNSS-derived global ionosphere maps for different solar activity levels: case studies for years 2014 and 2018. *GPS Solut.*, 25, 103. DOI: 10.1007/s10291-021-01142-x.

Wilgan, K., Hurter, F., Geiger, A. et al. (2017). Tropospheric refractivity and zenith path delays from least-squares collocation of meteorological and GNSS data. *J. Geod.*, 91, 117–134. DOI: 10.1007/s00190-016-0942-5.

Wilgan, K., and Geiger, A. (2019). High-resolution models of tropospheric delays and refractivity based on GNSS and numerical weather prediction data for alpine regions in Switzerland. *J. Geod.*, 93, 819–835. DOI: 10.1007/s00190-018-1203-6.

Yang, H., Hernandez-Pajares, M., Jarmolowski, W. et al. (2022). Systematic Detection of Anomalous Ionospheric Perturbations Above LEOs From GNSS POD Data Including Possible Tsunami Signatures. IEEE Trans. Geosci. *Remote Sens.*, 60, 1–23. DOI: 10.1109/TGRS.2022.3182885.

Yuan, P., Hunegnaw, A., Alshawaf et al. (2021). Feasibility of ERA5 integrated water vapor trends for climate change analysis in continental Europe: An evaluation with GPS (1994–2019) by considering statistical significance. *Remote Sens. Environ.*, 260, 112416. DOI: 10.1016/j.rse.2021.112416.

Zajdel, R., Kazmierski, K., and Sosnica, K. (2022). Orbital Artifacts in Multi-GNSS Precise Point Positioning Time Series. *J. Geophys. Res. Solid Earth*, 127. DOI: 10.1029/2021jb022994.